

Cosmic Lockdown: When Decoherence Saves the Universe from Tunneling

Robson Christie,^a Jaewoo Joo,^a Greg Kaplanek,^{b,c} Vincent Vennin,^d David Wands^e

^a*School of Mathematics and Physics, University of Portsmouth, PO1 3FX, United Kingdom*

^b*Department of Electrical Engineering and Computer Science, Syracuse University, NY 13210, USA*

^c*Institute for Quantum & Information Sciences, Syracuse University, NY 13210, USA*

^d*Laboratoire de Physique de l'Ecole Normale Supérieure, ENS, CNRS, Université PSL, Sorbonne Université, Université Paris Cité, 75005 Paris, France*

^e*Institute of Cosmology & Gravitation, University of Portsmouth, Dennis Sciama Building, Burnaby Road, Portsmouth, PO1 3FX, United Kingdom*

E-mail: robson.christie@port.ac.uk, jaewoo.joo@port.ac.uk, gkaplane@syr.edu,
vincent.vennin@phys.ens.fr, david.wands@port.ac.uk

ABSTRACT: We investigate how quantum decoherence influences the tunneling dynamics of quantum fields in cosmological spacetimes. Specifically, we study a scalar field in an asymmetric double-well potential during inflation, coupled to environmental degrees of freedom provided either by heavy spectator fields or by short-wavelength modes as they cross out the Hubble scale. This setup enables a systematic derivation of both Markovian and non-Markovian master equations, along with their stochastic unravelings, which we solve numerically. We find that, while decoherence is essential for suppressing quantum interference between vacua, its impact on the relative vacuum populations is limited. Fields heavier than the Hubble scale relax adiabatically toward the true vacuum with high probability, while lighter fields exhibit non-adiabatic enhancements of false-vacuum occupation. Once the system has decohered, quantum tunneling between vacua becomes strongly suppressed, effectively locking the system into the stochastically selected local minimum. This “cosmic lockdown” mechanism is a manifestation of the quantum Zeno effect: environmental monitoring stabilizes enhanced false-vacuum occupation for light fields by preventing them from tunneling.

Contents

1	Introduction	1
2	Markovian master equations	5
2.1	Four point system-bath interaction master equations	6
2.2	Stochastic inflation master equation	9
2.3	Spectator dynamics with bath decoherence and stochastic inflation	10
3	Numerical results: from kinetic to potential dominance	10
4	Late-time spectator dynamics with bath decoherence and stochastic inflation	15
5	Summary	17
6	Data and code availability	17
7	Acknowledgements	17
A	Master equations and bath correlators in de Sitter	22
A.1	Single-oscillator bath in de Sitter	22
A.2	Continuous oscillator bath spectra	24
B	Coarse graining in k-space and stochastic inflation	27
C	Adiabatic theorem for an oscillator in de Sitter	30
D	Additional simulations	30
D.1	$\phi^2\chi^2$ four point interactions	30
D.2	Non-Markovian single spectator environment	31

1 Introduction

The stability of vacuum states in quantum field theory has long been a concern in cosmology. Scalar fields with multiple minima naturally give rise to the possibility of false vacua, in which the universe becomes trapped in a metastable state with relatively higher energy density. The modern understanding of false vacuum decay began with the work of Coleman and Callan [1, 2], who showed how tunneling between vacua can be described semi-classically through instanton solutions in field theory. Their formalism was later generalised to gravitational and cosmological settings, first by Coleman and De Luccia who demonstrated how gravitational effects can modify vacuum decay rates [3], and later by Hawking and Moss who analysed transitions in de Sitter space driven by thermal fluctuations over the potential barrier [4]. These results established a physical mechanism that could in principle have serious implications for the large-scale evolution of the universe. Related treatments of barrier crossing within the stochastic-inflation framework have also been explored more recently [5–8].

A further example comes from the Standard Model itself. The vacuum expectation value of the Higgs field defines the familiar electroweak vacuum, which gives masses to Standard Model particles and determines the structure of low-energy physics. If one assumes that no additional particles or interactions enter the theory up to very high energies, the renormalization-group flow of the Higgs quartic coupling is fixed by measured Standard Model parameters such as the Higgs mass and calculable loop corrections (dominated by the top quark). With these inputs, the Higgs' quartic coupling becomes negative and its effective potential develops a second, deeper minimum at very large field values [9–13]. In the Standard Model, the associated tunneling rate to the deeper vacuum is typically calculated to be extraordinarily small, so that the electroweak vacuum lifetime vastly exceeds the age of the universe [10, 14–16] (see however [17]). Nevertheless, it can be unsettling to realize that our universe could, in principle, transition abruptly into a radically different state—one in which the structure of matter and the forces governing it are altered, effectively erasing the world as we know it.

Reassuringly, the parameters of our universe make such an event extraordinarily unlikely. However, even if the parameters suggested a greater tunneling probability, it would still be important to recognize that these calculations are highly idealized. They are typically performed in Euclidean signature and treat the quantum fields as perfectly isolated, so all evolution occurs simply under a Hamiltonian (and so is unitary). However, in realistic cosmological settings, all fields inevitably interact with a multitude of environmental degrees of freedom, including gravitational perturbations, other matter fields, and possibly hidden sectors. Importantly, in a universe dominated by gravity, its universal coupling ensures that no field is entirely isolated in cosmology. This motivates the central question of this work: how decoherence induced by environmental interactions modifies the standard semiclassical picture of false-vacuum decay and whether it can suppress coherent transitions to influence the fate of cosmological vacua. It also raises the issue of vacuum selection, which instanton calculations often provide little insight about.

To address these questions, we instead study here a model of the density matrix for a real scalar field ϕ placed in pure de Sitter space, where the line element is

$$ds^2 = -dt^2 + a^2(t)d\mathbf{x}^2 \quad \text{with scale factor } a(t) = e^{Ht} \quad (1.1)$$

where H is the Hubble scale and cosmic time t is related to the number of e -folds through

$$N = Ht. \quad (1.2)$$

The main feature of our setup is that the field evolves in a potential $V(\phi)$ with two inequivalent vacua while additionally interacting with an environment, allowing us to capture the effects of decoherence on vacuum dynamics. Throughout we model the environment as a continuum of massive spectator scalars X^a coupled locally to ϕ via quartic interactions of the form $\phi^{4-k}(X^a)^k$ with $k = 1, 2, 3$; in the main text we focus on a $\phi(X^a)^3$ coupling, while the $\phi^3 X^a$ and $\phi^2(X^a)^2$ cases and their corresponding master equations are discussed in App. A. Throughout we consider the quartic potential

$$V(\phi) = -\frac{1}{2}\mu^2\phi^2 + \frac{2}{3}\beta_3\mu\phi^3 + \frac{1}{4}(\beta_4^2 - \beta_3^2)\phi^4, \quad (1.3)$$

see Figure 1, with

$$\mu > 0, \quad \beta_4 > 0, \quad \beta_4^2 > \beta_3^2, \quad (1.4)$$

so that the potential is bounded from below. This quartic admits a local maximum at the origin,

$$\phi_M = 0, \quad (1.5)$$

and two nondegenerate minima at

$$\phi_T = -\frac{\mu}{\beta_4 - \beta_3}, \quad \phi_F = +\frac{\mu}{\beta_4 + \beta_3}. \quad (1.6)$$

Evaluating the potential at the minima gives

$$V(\phi_T) = -\frac{3\beta_4 - \beta_3}{12(\beta_4 - \beta_3)^3} \mu^4, \quad V(\phi_F) = -\frac{3\beta_4 + \beta_3}{12(\beta_4 + \beta_3)^3} \mu^4, \quad (1.7)$$

so the vacuum-energy splitting is

$$\Delta V \equiv V(\phi_T) - V(\phi_F) = \frac{4\beta_3\beta_4^3}{3(\beta_4^2 - \beta_3^2)^3} \mu^4. \quad (1.8)$$

For the parameter range (1.4), $\Delta V > 0$, hence ϕ_T is the true vacuum and ϕ_F is the false vacuum in the regime of interest. The curvature at the barrier is fixed by

$$V''(\phi_M) = -\mu^2, \quad (1.9)$$

so μ directly quantifies the instability scale. The effective masses governing small fluctuations about the two vacua follow from (1.3) and (1.6):

$$m_F^2 = V''(\phi_F) = \mu^2 \left(1 + \frac{\beta_4 + \beta_3}{\beta_4 - \beta_3} \right), \quad m_T^2 = V''(\phi_T) = \mu^2 \left(1 + \frac{\beta_4 - \beta_3}{\beta_4 + \beta_3} \right). \quad (1.10)$$

For $\beta_4^2 > \beta_3^2$ one has

$$m_T^2 > m_F^2, \quad (1.11)$$

so the true vacuum has a larger effective mass. In the near-symmetric limit $|\beta_3| \ll \beta_4$,

$$\Delta V \simeq \frac{4\beta_3}{3\beta_4^3} \mu^4 \left[1 + \mathcal{O}\left(\frac{\beta_3}{\beta_4}\right)^2 \right], \quad (1.12)$$

and the two vacua become nearly degenerate, which is useful for testing environment-induced decoherence in a controlled small-splitting regime.

We can see both effective masses are proportional to μ the mass scale of the potential, to quantify adiabaticity we define the dimensionless parameter

$$\tilde{\mu} \equiv \frac{\mu}{H}. \quad (1.13)$$

Physically $\tilde{\mu}$ compares the growth rate of the effective inverted oscillator at the barrier top to the Hubble rate (see Appendix C for related illustrative example). We also couple to other spectator fields, schematically represented by additional scalar fields χ via four-point interactions of the form

$$\mathcal{L}_{\text{int}} = \underline{\lambda}_1 \phi^3 \chi + \underline{\lambda}_2 \phi^2 \chi^2 + \underline{\lambda}_3 \phi \chi^3 \quad \text{with } \underline{\lambda}_j > 0. \quad (1.14)$$

Here $\underline{\lambda}_j$ are bare dimensionless couplings in the action (whereas renormalized couplings λ_j appear in the dynamical equations instead). Our focus in the main text will be on the third $\phi \chi^3$ interaction, although we explore all interactions in Appendix A.

All fields are treated as spectators in de Sitter space, so backreaction on the geometry is neglected. Because the dynamics in de Sitter are so complicated we make the simplification of studying only the

constant $\mathbf{k} = \mathbf{0}$ mode of the field (see eq. (2.17) for definition), and leave further investigation of scale dependence to future work.

Our setup allows us to derive both Markovian and non-Markovian master equations that describe the reduced dynamics of the scalar field in a quartic potential. Since analytic solutions of these equations, even just for the zero mode, are intractable, we solve them numerically using a truncated Fock basis to explore how environmental interactions influence vacuum selection in an inflationary background. Appendix C provides an illustrative and analytically tractable quadratic parametric oscillator example. These master equations provide an ensemble-averaged description of the reduced density matrix, which captures the coarse-grained evolution in phase space, represented by the Wigner function. This is contrasted in our results with the dynamics of individual stochastic trajectories, which can exhibit more varied behavior. In this sense, master equations, in particular Lindblad, offer a natural description of vacuum selection under decoherence at the level of averaged, physically observable quantities.

Our analysis reveals several key results:

- First, the adiabaticity parameter $\tilde{\mu}$ controls the relative vacuum populations. If the Hubble rate is small compared to the mass scale set by the potential, the evolution is adiabatic: the field follows the instantaneous ground state and becomes localized in the true vacuum at late times. By contrast, when $\tilde{\mu}$ is sufficiently small, the evolution is rapid and non-adiabatic, and the system relaxes to a mixed state with comparable populations in both minima, with a non-adiabatic enhancement of the false-vacuum occupation.
- Second, we find that decoherence itself doesn't have much influence on *which* vacuum is chosen. Introducing a nonzero coupling to the environment ($\lambda \neq 0$) does not significantly affect the relative probability of ending in the true or false vacuum. Instead, the principal role of decoherence is to suppress quantum interference between vacua, ensuring that once a vacuum is selected the system cannot tunnel through the barrier.
- Third, the time-dependence of the de Sitter background means that the potential acquires a growing prefactor with time (coming from $\sqrt{-g}$ required on the grounds of covariance), which increases the energetic separation between minima and sharpens the wells in phase space at late times. This stretching of the potential in phase space helps to reinforce the outcome of vacuum selection.
- Fourth, at late times the system has decohered into a definite local minimum, quantum tunneling between vacua is strongly suppressed. Even if the field settles into a false vacuum, continuous environmental “monitoring” or “measurement” induces a quantum Zeno effect [18, 19], suppressing any subsequent tunneling back to the true vacuum. In this sense, decoherence gives rise to something we call a *cosmic lockdown* mechanism, stabilizing whichever vacuum the system has reached and preventing further evolution through tunneling.

These findings build on earlier work showing that scalars, gravitons and other environmental degrees of freedom induce decoherence in cosmology [20–55] which are more closely related to semi-classical instanton studies first mentioned. Our minimal toy model shows how environmental interactions can alter the standard picture of false-vacuum decay. Unlike [33], which assumes the system starts in the false vacuum, we consider an initial state in the instantaneous ground state, which is delocalized across both vacua.

2 Markovian master equations

In this section we present the cosmological master equations, together with their stochastic unravelings, that underpin the remainder of this work. We work in e -fold time N .

In the absence of any environment, the state vector $|\psi\rangle$ obeys the Schrödinger equation

$$\partial_N |\psi\rangle = -i\hat{K}_S(N)|\psi\rangle, \quad (2.1)$$

which is equivalently written for the density operator $\hat{\rho} = |\psi\rangle\langle\psi|$ as the von Neumann equation

$$\partial_N \hat{\rho} = -i[\hat{K}_S(N), \hat{\rho}]. \quad (2.2)$$

In the remainder of the paper we specialise to the effective Hamiltonian for the zero mode of the spectator field, which is derived from first principles in §2.1. Written in e -fold time this Hamiltonian takes the form

$$\hat{K}_S(N) = \frac{e^{-3N}}{2H\text{vol}} \hat{\pi}_\phi^2 + \frac{e^{3N}\text{vol}}{H} \left[-\frac{1}{2}\mu^2\hat{\phi}^2 + \frac{2}{3}\beta_3\mu\hat{\phi}^3 + \frac{1}{4}(\beta_4^2 - \beta_3^2)\hat{\phi}^4 \right], \quad (2.3)$$

where the comoving volume factor vol is later defined in Eq. (2.20) and $\hat{\phi}$ is the field operator with canonical momentum¹

$$\hat{\pi}_\phi = a^3 H \partial_N \hat{\Phi}_0 \quad \text{with} \quad [\hat{\phi}, \hat{\pi}_\phi] = i. \quad (2.4)$$

Across all simulations we fix the parameters

$$\mu = 0.5 \text{ [mass}^{+1}\text{]}, \quad \beta_3 = 0.025, \quad \beta_4 = 0.13, \quad \text{vol} = 1 \text{ [mass}^{-3}\text{]} \quad (2.5)$$

for ease of comparison. Our choice of these specific numerical values is arbitrary; they are chosen so that, near the conventional origin $N = 0$, the potential contribution $e^{3N}V(\phi)$ is comparable in magnitude to the kinetic contribution $e^{-3N}\pi_\phi^2$ in the effective Hamiltonian (2.3). This entails no loss of generality, because a shift of the e -folding origin,

$$N = N' + \Delta, \quad (2.6)$$

can be absorbed into a redefinition of parameters:

$$\mu' = e^{\frac{3}{2}\Delta} \mu, \quad \beta'_3 = e^{\frac{3}{2}\Delta} \beta_3, \quad \beta'_4 = e^{\frac{3}{2}\Delta} \beta_4, \quad \lambda'^2 = e^{\frac{27}{2}\Delta} \lambda^2. \quad (2.7)$$

With these rescalings, both the potential term $e^{3N}V(\phi)$ and the decoherence terms (via the definition of λ in Eq. (2.34)) retain exactly the same functional dependence when written in terms of the shifted time N' . Equivalently, if the kinetic and potential contributions are mismatched at the reference point $N = 0$ for some choice of Lagrangian parameters, one can choose Δ (and work with N' and the primed couplings) so that the two contributions become comparable near the new origin $N' = 0$, without changing the underlying physics.

To incorporate decoherence and dissipation from a memoryless environment we generalize (2.2) to a Gorini-Kossakowski-Lindblad-Sudarshan (GKLS) [56, 57] master equation of the form

$$\partial_N \hat{\rho} = -i[\hat{K}_S(N), \hat{\rho}] - \frac{1}{2} \sum_{\alpha} \gamma_{\alpha}(N) [\hat{L}_{\alpha}, [\hat{L}_{\alpha}, \hat{\rho}]], \quad (2.8)$$

¹If $\Pi_{\mathbf{k}} = e^{3N}H\partial_N\Phi_{\mathbf{k}}$, then one has the standard relation $[\Phi_{\mathbf{k}}, \Pi_{\mathbf{q}}] = i\delta^{(3)}(\mathbf{k} + \mathbf{q})$, which implies $[\Phi_0, \Pi_0] = i \cdot \text{vol}$. Translating to ϕ gives Eq. (2.4), and explains the volume factor in the definition of the canonical momentum.

where the \hat{L}_α are Hermitian Lindblad operators and $\gamma_\alpha(N) \geq 0$ are time-dependent decoherence rates.

Two normalised Itô stochastic Schrödinger equations (SSEs) [58, 59] that unravel (2.8) can be written as

$$\begin{aligned} d|\psi\rangle = -i\hat{K}_S(N)|\psi\rangle dN - \frac{1}{2} \sum_\alpha \gamma_\alpha(N) \left(\hat{L}_\alpha - \langle \hat{L}_\alpha \rangle \right)^2 |\psi\rangle dN \\ + \sum_\alpha \sqrt{\gamma_\alpha(N)} (\hat{L}_\alpha - \langle \hat{L}_\alpha \rangle) |\psi\rangle dW_\alpha, \end{aligned} \quad (2.9)$$

$$d|\psi\rangle = -i\hat{K}_S(N)|\psi\rangle dN - \frac{1}{2} \sum_\alpha \gamma_\alpha(N) \hat{L}_\alpha^2 |\psi\rangle dN + i \sum_\alpha \sqrt{\gamma_\alpha(N)} \hat{L}_\alpha |\psi\rangle dW_\alpha, \quad (2.10)$$

where the dW_α are independent real Wiener increments with $\mathbb{E}[dW_\alpha] = 0$ and $\mathbb{E}[dW_\alpha dW_\beta] = dN \delta_{\alpha\beta}$. Despite their different forms, ensemble averages of the pure-state trajectories governed by Eqs. (2.9) and (2.10) both reproduce the same density-matrix evolution (2.8). Their interpretations, however, are quite different.

The SSE in Eq. (2.9) is a nonlinear, norm-preserving equation in which the noise couples through the fluctuation operators $\hat{L}_\alpha - \langle \hat{L}_\alpha \rangle$. It corresponds to an effective environmental monitoring with system-bath interaction Hamiltonian

$$\hat{H}_{\text{int}} = \sum_\alpha \hat{L}_\alpha \otimes \hat{B}_\alpha, \quad (2.11)$$

together with Markovian interaction-picture bath correlators

$$\langle \hat{B}_{\alpha_1}(t) \hat{B}_{\alpha_2}(t') \rangle = \delta_{\alpha_1 \alpha_2} \gamma_{\alpha_1}(N) \delta(t - t'), \quad (2.12)$$

which encode the decoherence rates $\gamma_\alpha(N) \geq 0$. In this picture Eq. (2.9) describes continuous measurement or bath-induced localization at the level of individual trajectories. By contrast, the SSE in Eq. (2.10) is linear and can be viewed as a Schrödinger equation with a random, Hermitian perturbation to the system Hamiltonian $\hat{H}_{\text{stoch}} = \sum_\alpha \sqrt{\gamma_\alpha(N)} \hat{L}_\alpha dW_\alpha$ [60].

2.1 Four point system-bath interaction master equations

As discussed in §1, we study a de Sitter analogue of the Caldeira-Leggett model [60, 61], in which a system \mathcal{S} interacts with an environment \mathcal{E} through an overall action of the form

$$S = S_{\mathcal{S}} + S_{\mathcal{E}} + S_{\text{int}}. \quad (2.13)$$

The system we take to be a real scalar field Φ such that

$$S_{\mathcal{S}} = \int dt a^3 \int d^3 \mathbf{x} \left[\frac{1}{2} \dot{\Phi}^2 - \frac{1}{2a^2} |\nabla \Phi|^2 - V(\Phi) \right], \quad (2.14)$$

which self-interacts via the potential from eq. (1.3). We also consider a family of massive real scalar fields $\{X^a\}$ each with their own distinct mass m_a such that

$$S_{\mathcal{E}} = \sum_a \int dt a^3 \int d^3 \mathbf{x} \left[\frac{1}{2} (\dot{X}^a)^2 - \frac{1}{2a^2} |\nabla X^a|^2 - \frac{1}{2} m_a^2 (X^a)^2 \right]. \quad (2.15)$$

Finally, we assume that the system field Φ linearly couples to all environmental fields X^a through an interaction of the form

$$S_{\text{int}} = -\lambda \sum_a g_a \int dt a^3 \int d^3 \mathbf{x} \Phi (X^a)^3 \quad (2.16)$$

with distinct dimensionless couplings $\{g_a\}$ and another bare dimensionless coupling λ used for later bookkeeping. In Appendix A we explore more general quartic (four-point) interactions between system and environment, see eq. (A.3).

Our goal will be to simplify the theory by use of the isotropy of de Sitter space, where we Fourier transform the fields to momentum space using the convention

$$\Phi(t, \mathbf{x}) = \int \frac{d^3\mathbf{k}}{(2\pi)^3} \Phi_{\mathbf{k}}(t) e^{i\mathbf{k}\cdot\mathbf{x}} \quad \text{and} \quad X^a(t, \mathbf{x}) = \int \frac{d^3\mathbf{k}}{(2\pi)^3} X_{\mathbf{k}}^a(t) e^{i\mathbf{k}\cdot\mathbf{x}}. \quad (2.17)$$

The equations of motion for the fields are then given by²

$$\ddot{\Phi}_{\mathbf{k}} + 3H\dot{\Phi}_{\mathbf{k}} + \frac{k^2}{a^2}\Phi_{\mathbf{k}} + [V'(\Phi)]_{\mathbf{k}} + \lambda \sum_a g_a [(X^a)^3]_{\mathbf{k}} = 0, \quad (2.18)$$

$$\ddot{X}_{\mathbf{k}}^a + 3H\dot{X}_{\mathbf{k}}^a + \left(\frac{k^2}{a^2} + m_a^2 \right) X_{\mathbf{k}}^a + 3\lambda g_a [\Phi(X^a)^2]_{\mathbf{k}} = 0. \quad (2.19)$$

We consider the constant $\mathbf{k} = \mathbf{0}$ mode of each of the above fields, which simplifies (2.13) to

$$S \simeq \text{vol} \int dt a^3 \left\{ \frac{\dot{\Phi}_{\mathbf{0}}^2}{2\text{vol}^2} - V \left(\frac{\Phi_{\mathbf{0}}}{\text{vol}} \right) + \sum_a \left[\frac{(\dot{X}_{\mathbf{0}}^a)^2 - m_a^2 (X_{\mathbf{0}}^a)^2}{\text{vol}^2} - \lambda \frac{g_a \Phi_{\mathbf{0}} (X_{\mathbf{0}}^a)^3}{\text{vol}^4} \right] \right\} + (\text{non-zero modes}) \quad (2.20)$$

where a constant (comoving) volume factor $\text{vol} := (2\pi)^3 \delta^{(3)}(\mathbf{0})$ is included on dimensional grounds³. In this limit we neglect all gradient terms, or equivalently take $k/aH \ll 1$ in the equations of motion. This approximation is easily justified on super-Hubble scales (at late times), but is a drastic approximation on sub-Hubble scales, since (i) the gradient terms dominate at early times and (ii) the mode-to-mode couplings (via the Φ^3 , Φ^4 and $\Phi(X^a)^3$ interactions) become important. In subsection 2.2 we will replace the zero-mode truncation above with a Hubble-patch average, providing a coarse-grained description of dynamics on Hubble scales; here however, we content ourselves with this simpler treatment. Note that this approximation parallels that of Hawking and Moss [4] of vacuum decay in de Sitter space, where the transition is governed entirely by the homogeneous mode due to the suppression of spatial gradients.

We next assume that there are infinitely many X^a fields, where the discretely many masses m_a are so densely distributed such that we replace them with a continuum of masses m such that

$$m_a \rightarrow m \quad \text{and} \quad \sum_a g_a \rightarrow \frac{1}{\mu} \int_0^\infty dm G(m) \quad (2.21)$$

where μ is the reference mass scale from the potential defined in (1.3). Because the frequencies are continuous we replace the label on the fields such that $X^a \rightarrow X(m)$ and the couplings become $g_a \rightarrow G(m)$, giving

$$S \simeq \text{vol} \int dt a^3 \left\{ \frac{\dot{\Phi}_{\mathbf{0}}^2}{2\text{vol}^2} - V \left(\frac{\Phi_{\mathbf{0}}}{\text{vol}} \right) + \int_0^\infty \frac{dm}{\mu} \left[\frac{\dot{X}_{\mathbf{0}}^2(m) - m^2 X_{\mathbf{0}}^2(m)}{2\text{vol}^2} - \lambda \frac{G(m) \Phi_{\mathbf{0}} X_{\mathbf{0}}^3(m)}{\text{vol}^4} \right] \right\}. \quad (2.22)$$

²We use standard notation where $[(X^a)^3]_{\mathbf{k}} = \int \frac{d\mathbf{k}_1}{(2\pi)^3} \int \frac{d\mathbf{k}_2}{(2\pi)^3} \int \frac{d\mathbf{k}_3}{(2\pi)^3} (2\pi)^3 \delta(\mathbf{k}_1 + \mathbf{k}_2 + \mathbf{k}_3 - \mathbf{k}) X_{\mathbf{k}_1}^a X_{\mathbf{k}_2}^a X_{\mathbf{k}_3}^a$ is the Fourier transform of $(X^a)^3$.

³In a finite volume the momentum integral becomes a discrete sum $\int d^3\mathbf{k} \rightarrow \frac{1}{\text{vol}} \sum_{\mathbf{k}}$.

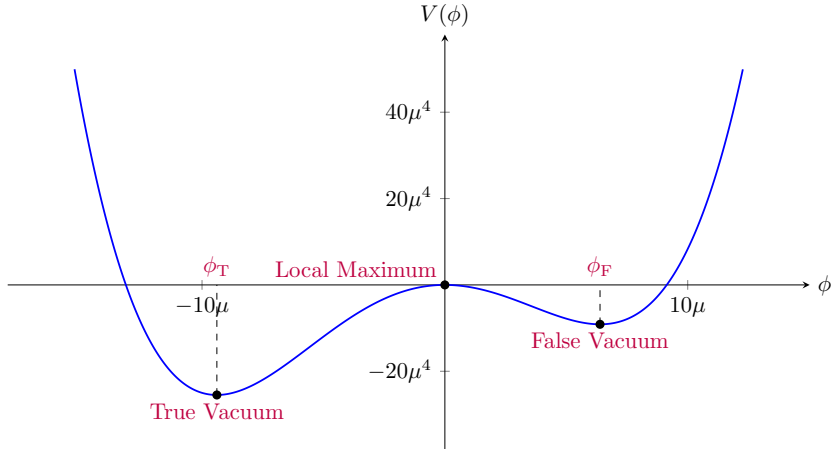


Figure 1: Potential $V(\phi)$ from (1.3) for the parameter choices $\beta_3 = 0.025$ and $\beta_4 = 0.13$.

We then rescale the fields such that

$$\phi = \frac{\Phi_0}{\text{vol}} , \quad \chi_m = \frac{X_0(m)}{\text{vol}} . \quad (2.23)$$

We switch on the coupling $\underline{\lambda}$ in the system-environment interaction at time t_0 , and choose the spectral density $G(m)$ to be

$$G(m) = \left(\frac{m}{\mu} \right)^{\frac{3}{2}} e^{-\frac{3m}{2\Lambda}} , \quad (2.24)$$

which compensates the mass scaling of the correlators of the homogeneous bath modes $X_0(m)$ and is precisely the choice that makes the ΦX^3 channel yield a time-local (Markovian) master equation; see Appendix A for the explicit calculation. The cutoff Λ is physically reasonable, since the system should only couple efficiently to environmental fields of comparable mass, while very heavy modes ($m \gg \Lambda$) can be integrated out in the Wilsonian sense and simply renormalise the self-interaction parameters in $V(\Phi_0/\text{vol})$. In Appendix A we also show how starting from a single massive environmental scalar with generic quartic couplings $\Phi^{4-k} X^k$ and promoting X to a continuum weighted by suitable powers of the same spectral density leads to Markovian master equations for $k = 1, 2, 3$, each with a different Lindblad structure.

The total Lagrangian L is defined by $S = \int dt L$, which gives

$$L(t) = \text{vol} \cdot a^3 \left\{ \frac{1}{2} \dot{\phi}^2 - V(\phi) - \frac{1}{\mu} \int_0^\infty dm \left[\frac{1}{2} \dot{\chi}_m^2 - \frac{1}{2} m^2 \chi_m^2 + \underline{\lambda} G(m) \phi \chi_m^3 \right] \right\} , \quad (2.25)$$

where the homogeneous zero mode $\phi(N)$ serves as the system (with dimensions of mass⁺¹), while the continuum of heavy spectator zero modes $\{\chi_m(N)\}$ acts as the environment (also with dimensions of mass⁺¹ in our conventions). We assume that these spectator modes begin in their ground state in the infinite past.

The potential $V(\phi)$ in (1.3) is asymmetric and always admits a false vacuum, as shown in Figure 1. In the main text we specialise to the $\phi\chi^3$ coupling, which, after renormalisation of the bare coupling, yields a purely decohering GKLS master equation with Lindblad operator proportional to $\hat{\phi}$; see

Appendix A for details. Within the general notation of (2.8) this corresponds to a master equation of the form

$$\partial_N \hat{\rho} = -i[\hat{K}_S(N), \hat{\rho}] - \frac{1}{2}\Gamma_\phi(N)[\hat{\phi}, [\hat{\phi}, \hat{\rho}]], \quad \text{with} \quad \Gamma_\phi(N) = \frac{131\pi\lambda^2 e^{6N}}{256\mu^5 \text{vol}}. \quad (2.26)$$

A convenient normalised nonlinear SSE of the type (2.9) that unravels (2.26) is

$$d|\psi\rangle = -i\hat{K}_S|\psi\rangle dN - \frac{1}{2}\Gamma_\phi(N)(\hat{\phi} - \langle\hat{\phi}\rangle)^2|\psi\rangle dN + \sqrt{\Gamma_\phi(N)}(\hat{\phi} - \langle\hat{\phi}\rangle)|\psi\rangle dW_\phi, \quad (2.27)$$

where dW_ϕ is a real Wiener increment. Ensemble averages of these pure state trajectories over noise realisations yield the solution of the $\hat{\phi}$ -Lindblad equation (2.26). This dynamics describes pure dephasing and localization in the $\hat{\phi}$ basis induced by the χ_m environment.

2.2 Stochastic inflation master equation

Coupling to an external bath is not the only mechanism that generates open-system dynamics. In de Sitter space, quantum field modes are continually stretched by the cosmic expansion. Coarse-graining over a physical patch of radius $(\sigma H)^{-1}$ with $\sigma \ll 1$ defines an effective long-wavelength field, while modes crossing the coarse-graining scale act as stochastic sources that randomly kick the field value with variance $H^2/4\pi^2$, as described in App. B, provided the field mass is small compared to the Hubble scale [62–66]. This framework, known as *stochastic inflation*, describes the coarse-grained (over a Hubble patch) dynamics of a light field and its canonically conjugate momentum through the Langevin process

$$d\phi = \frac{e^{-3N}}{\text{vol } H} \pi_\phi dN + \frac{H}{2\pi} dW, \quad (2.28)$$

$$d\pi_\phi = -\frac{\text{vol } e^{3N}}{H} V'(\phi) dN. \quad (2.29)$$

In App. B we show that there exists a unique normalised SSE

$$d|\psi\rangle = -i\hat{K}_S(N)|\psi\rangle dN - \frac{1}{2}\Gamma_\pi \hat{\pi}_\phi^2 |\psi\rangle dN - i\sqrt{\Gamma_\pi} \hat{\pi}_\phi |\psi\rangle dW_\pi, \quad \text{with} \quad \Gamma_\pi = \frac{H^2}{4\pi^2} \quad (2.30)$$

which, at the level of field expectation values, reproduces the Langevin equations (2.28) and (2.29):

$$d\langle\hat{\phi}\rangle = \frac{e^{-3N}}{\text{vol } H} \langle\hat{\pi}_\phi\rangle dN + \frac{H}{2\pi} dW, \quad (2.31)$$

$$d\langle\hat{\pi}_\phi\rangle = -\frac{\text{vol } e^{3N}}{H} \langle V'(\hat{\phi}) \rangle dN. \quad (2.32)$$

For a double-well potential, these relations describe the stochastic dynamics of the homogeneous component of a test field in a quasi-de Sitter background, provided that the characteristic field mass scale μ remains small compared to the Hubble rate. In the present work we identify this coarse-grained long-wavelength field, averaged over a Hubble patch, with the zero mode of the spectator field used in Sec. 2.1, so that both the bath-induced GKLS channel and the stochastic-inflation channel act consistently on the same effective degree of freedom.

Averaging the SSE (2.30) over noise realisations yields the GKLS equation with a single $\hat{\pi}_\phi$ Lindblad term,

$$\partial_N \hat{\rho} = -i[\hat{K}_S(N), \hat{\rho}] - \frac{1}{2}\Gamma_\pi [\hat{\pi}_\phi, [\hat{\pi}_\phi, \hat{\rho}]]. \quad (2.33)$$

Here dW_π is a real Wiener increment. The SSE (2.30) can be viewed as a Schrödinger equation with a random, Hermitian Hamiltonian perturbation proportional to $\hat{\pi}_\phi$. Equivalently, since $\hat{\pi}_\phi$ generates translations, it describes a random translation of the state along $\hat{\phi}$. In other words, the evolution is unitary but driven by stochastic Hamiltonian noise, and it reproduces the standard stochastic-inflation Langevin dynamics at the level of expectation values.

2.3 Spectator dynamics with bath decoherence and stochastic inflation

We combine the bath-induced decoherence derived in App. A (from the $\phi\chi^3$ interaction) with the stochastic-inflation contribution of App. B to obtain a single GKLS equation for the spectator field. The combined effects of environmental interactions and stochastic inflation have been discussed in stochastic variable formulations in [67, 68], the formulation we present here is quite different in providing a GKLS master equation and explicit pure-state unravelings.

Throughout this subsection we assume the light-field regime $\tilde{\mu} \ll 1$ required for stochastic inflation. The resulting GKLS equation is

$$\partial_N \hat{\rho} = -i[\hat{K}_S(N), \hat{\rho}] - \frac{131\pi\lambda^2 e^{6N}}{512\mu^5 \text{vol}} [\hat{\phi}, [\hat{\phi}, \hat{\rho}]] - \frac{H^2}{8\pi^2} [\hat{\pi}_\phi, [\hat{\pi}_\phi, \hat{\rho}]], \quad (2.34)$$

which governs the coarse-grained dynamics of the spectator field in de Sitter when both the χ_m bath and stochastic coarse-graining effects are included. In the notation of (2.8) this corresponds to two Lindblad operators,

$$\hat{L}_1 \propto \hat{\phi}, \quad \hat{L}_2 \propto \hat{\pi}_\phi, \quad (2.35)$$

with decoherence rates proportional to $\lambda^2 e^{6N}$ and H^2 , respectively.

In order to see trajectory-wise effects such as localization and random translations when both channels are present, we unravel (2.34) with a normalised Itô Stochastic Schrödinger Equation (SSE) [58, 60] that combines the structures of (2.27) and (2.30):

$$\begin{aligned} d|\psi\rangle = & -i\hat{K}_S|\psi\rangle dN - \frac{131\pi\lambda^2 e^{6N}}{512\mu^5 \text{vol}} (\hat{\phi} - \langle\hat{\phi}\rangle)^2 |\psi\rangle dN - \frac{H^2}{8\pi^2} \hat{\pi}_\phi^2 |\psi\rangle dN \\ & + \sqrt{\frac{131\pi\lambda^2 e^{6N}}{256\mu^5 \text{vol}}} (\hat{\phi} - \langle\hat{\phi}\rangle) |\psi\rangle dW_1 - \frac{iH}{2\pi} \hat{\pi}_\phi |\psi\rangle dW_2, \end{aligned} \quad (2.36)$$

where $dW_{1,2}$ are real Wiener increments with $\mathbb{E}[dW_i] = 0$ and $\mathbb{E}[dW_i dW_j] = dN \delta_{ij}$. Ensemble averages of these pure state trajectories over noise realisations yield the solution of the combined GKLS equation (2.34). In terms of the general structure in (2.9) and (2.10), (2.36) is the special case with two Lindblad operators $\hat{L}_1 \propto \hat{\phi}$ (treated in a nonlinear, measurement-like form) and $\hat{L}_2 \propto \hat{\pi}_\phi$ (treated as stochastic Hamiltonian noise), with the corresponding rates fixed by (2.34).

3 Numerical results: from kinetic to potential dominance

We solve the Hilbert-space dynamics introduced in the previous section numerically on the interval $N \in [-2, 1]$, which contains the *barrier switch-on* period during which the effective Hamiltonian transitions from kinetic-term dominance to potential dominance and non-adiabatic effects are most prominent. The initial state used in all simulations is the instantaneous ground state of \hat{K}_S at $N = -2$, shown in Fig. 2(a). We monitor the right-well occupation

$$P_{\text{false}}(N) \equiv \text{Tr}[\hat{\theta}_{\phi^+} \hat{\rho}(N)], \quad \hat{\theta}_{\phi^+} = \int_0^\infty d\phi |\phi\rangle \langle\phi|, \quad (3.1)$$

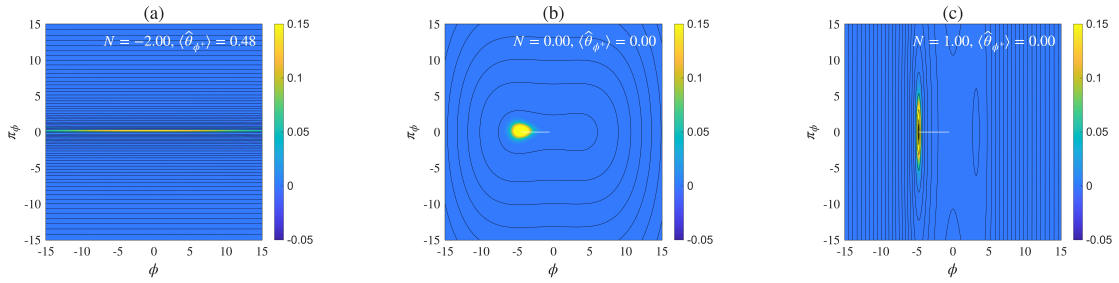


Figure 2: Adiabatic limit ($\tilde{\mu} \rightarrow \infty$). Wigner functions showing the instantaneous Hamiltonian (2.3) ground state at three snapshot times. Panel (a) is the instantaneous ground state at e-fold $N = -2$, which is the initial state used in every simulation in this paper. The black curves are equal-energy contours of $K_S(N)$. Axes are ϕ and π_ϕ . In-panel text reports the e -fold N and the false-vacuum projector expectation value $\langle \hat{\theta}_{\phi+} \rangle = \text{Tr}(\hat{\theta}_{\phi+}\hat{\rho}(N))$. The white line corresponds to the evolution prior to the snapshot of the phase-space expectation values $\langle \hat{\phi} \rangle$ and $\langle \hat{\pi}_\phi \rangle$. The sonified video corresponding to these plots is available [via this link](#) with sonification method described in [69].

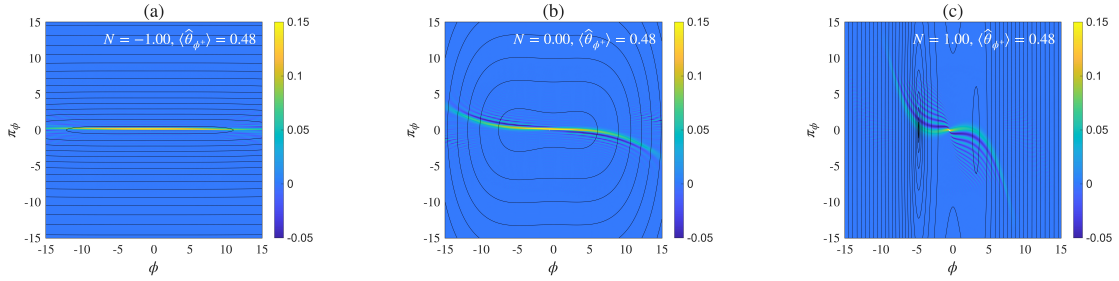


Figure 3: Schrödinger dynamics. Wigner functions for Hamiltonian evolution (2.1) without decoherence. The system is evolved unitarily from the instantaneous ground state at $N = -2$. Columns correspond to different snapshot times. Black curves are equal-energy contours of $K_S(N)$. Axes are ϕ and π_ϕ . In-panel text reports the e -fold N and the false-vacuum projector expectation value. The sonified video corresponding to these plots is available [via this link](#) with sonification method described in [69]. The white line corresponds to the prior evolution of the phase-space expectation values $\langle \hat{\phi} \rangle$ and $\langle \hat{\pi}_\phi \rangle$. The adiabaticity parameter used for this simulation is $\tilde{\mu} = 0.1$.

for which $P_{\text{false}}(N = -2) \approx 1/2$ due to kinetic dominance at the start. We also track the purity $\text{Tr}[\hat{\rho}(N)^2]$ and the Wigner function [70, 71]

$$W(\phi, \pi_\phi; N) = \int_{-\infty}^{\infty} d\xi \left\langle \phi - \frac{\xi}{2} \middle| \hat{\rho}(N) \middle| \phi + \frac{\xi}{2} \right\rangle e^{i\pi_\phi \xi}. \quad (3.2)$$

Figs. 2–5 and 7–9 compare Wigner functions across a range of dynamical scenarios with identical axes, ranges, and colour scales. The black curves show equal-energy contours of the time-dependent Hamiltonian $\hat{K}_S(N)$. Columns give snapshots at $N = -1, 0, 1$. Figure 6 collects false-vacuum occupation and purity for parameter sweeps in the GKLS dynamics.

At large N , phase-space squeezing requires an exponentially dense grid to resolve the wavefunction accurately, which in our current implementation limits simulations to $N \leq 1$. In the late-time regime ($N > 1$) the potential term $e^{3N}V$ dominates over the kinetic term $e^{-3N}\pi_\phi^2$, and decoherence is strong

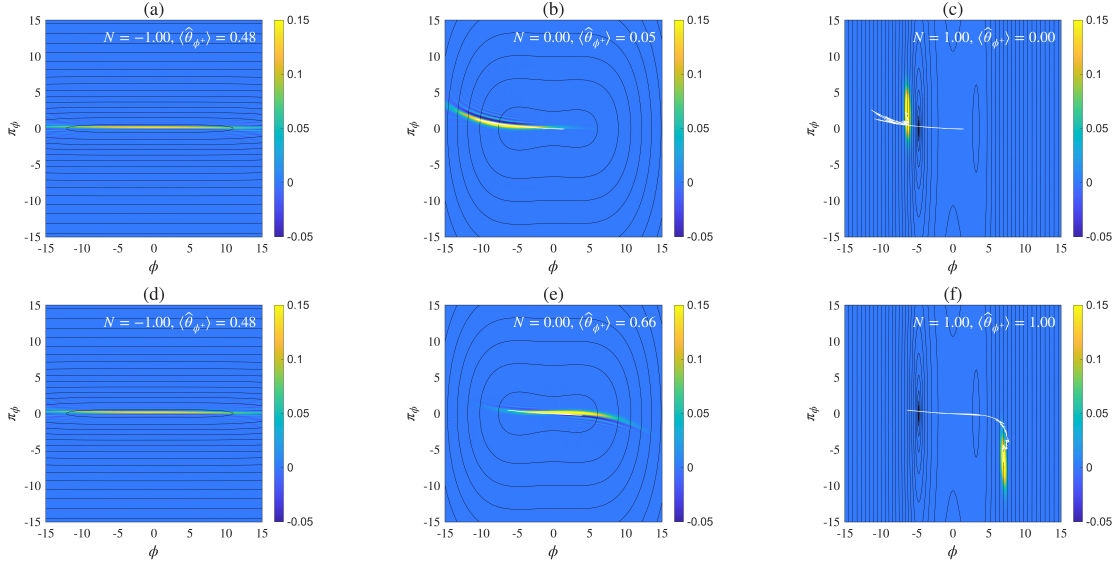


Figure 4: $\hat{L} \propto \hat{\phi}$ SSE dynamics, Wigner functions for the SSE evolution (2.27). The top row shows an SSE trajectory ending in the true vacuum, and the bottom row shows an SSE trajectory ending in the false vacuum. Columns correspond to different snapshot times. Black curves are equal-energy contours of $K_S(N)$. Axes are ϕ and π_ϕ . In-panel text reports the e -fold N and the false-vacuum projector expectation value. The sonified videos corresponding to these plots are available via these links: [true vacuum](#) and [false vacuum](#) with sonification method described in [69]. The white line corresponds to the prior evolution of the phase-space expectation values $\langle \hat{\phi} \rangle$ and $\langle \hat{\pi}_\phi \rangle$. The adiabaticity parameter used for this simulation is $\tilde{\mu} = 0.1$.

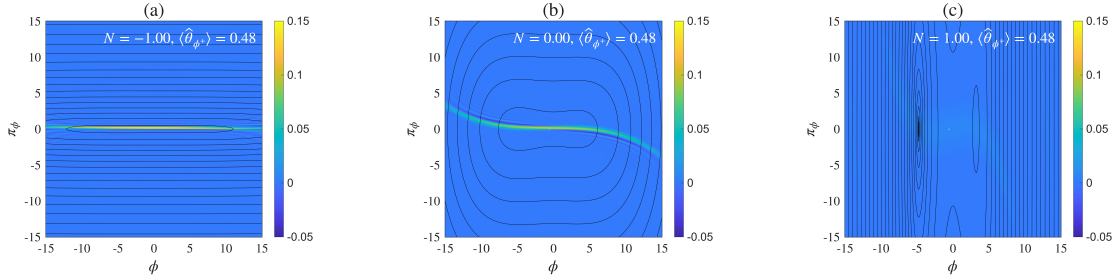


Figure 5: $\hat{L} \propto \hat{\phi}$ GKLS dynamics, Wigner functions for Lindblad evolution (2.26), with columns corresponding to different snapshot times. Black curves are equal-energy contours of $K_S(N)$. Axes are ϕ and π_ϕ . In-panel text reports the e -fold N and the false-vacuum projector expectation value. The sonified video corresponding to these plots is available [via this link](#) with sonification method described in [69]. The white line corresponds to the prior evolution of the phase-space expectation values $\langle \hat{\phi} \rangle$ and $\langle \hat{\pi}_\phi \rangle$. The adiabaticity parameter used for this simulation is $\tilde{\mu} = 0.1$.

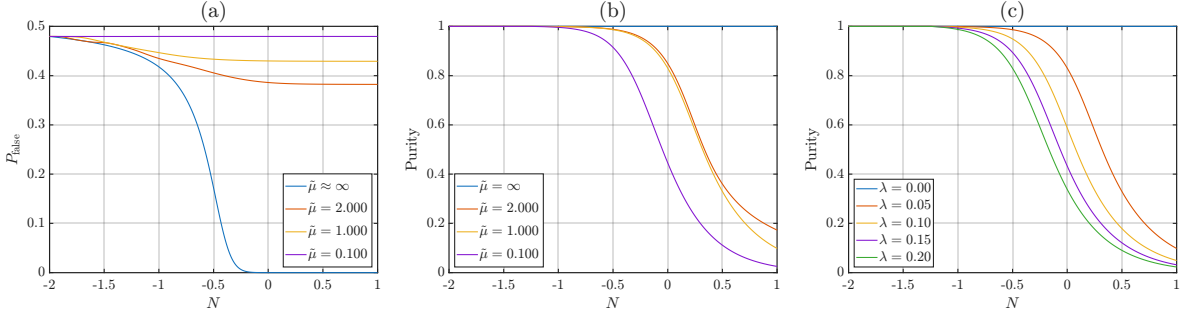


Figure 6: $\hat{L} \propto \hat{\phi}$ **GKLS dynamics**, Parameter-sweep comparison of right-well occupation and purity versus e -fold time N for the GKLS evolution (2.26). (a): adiabaticity $\tilde{\mu}$ sweep with dephasing strength $\lambda = 0.05$ showing $P_{\text{false}} \equiv \text{Tr} \left(\hat{\theta}_{\phi^+} \hat{\rho}(N) \right)$. (b): adiabaticity $\tilde{\mu}$ sweep with $\lambda = 0.05$ showing purity $P(N) = \text{Tr} \left[\hat{\rho}^2(N) \right]$. (c): λ sweep at fixed adiabaticity $\tilde{\mu} = 1$ showing purity $P(N)$. We also ran a λ sweep for P_{false} but found no differences in this observable between different λ values, as expected. All runs use the same initial state and potential.

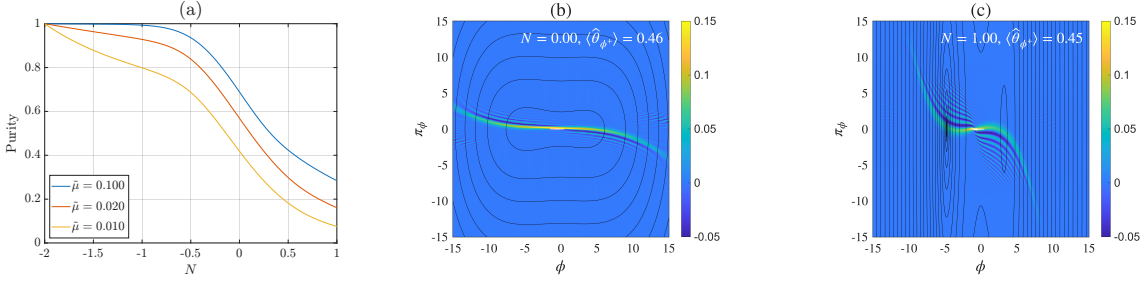


Figure 7: \hat{L}_{π_ϕ} **GKLS and SSE dynamics**, Panel (a) shows an adiabaticity $\tilde{\mu}$ sweep of the purity $P(N) = \text{Tr} \left[\hat{\rho}^2(N) \right]$ for the GKLS dynamics (2.33). Panels (b) and (c) show Wigner snapshots for the stochastic inflation SSE evolution (2.30). The sonified videos corresponding to these plots are available via [this link](#) with sonification method described in [69]. The white line corresponds to the prior evolution of the phase-space expectation values $\langle \hat{\phi} \rangle$ and $\langle \hat{\pi}_\phi \rangle$. The adiabaticity parameter used for panels (b) and (c) is $\tilde{\mu} = 0.1$.

($\propto e^{6N}$). In this limit, a strong-localization approximation gives an Arrhenius-type estimate for the stochastic over-the-barrier hopping rates between vacua, which we derive in the next section.

During the $N \in [-2, 1]$ simulation window, the adiabaticity parameter $\tilde{\mu}$ controls vacuum selection, as demonstrated in Fig. 6(a,b). We vary $\tilde{\mu}$ by fixing $\mu = 0.5$ and changing the Hubble rate, which keeps the initial state identical between runs; changing μ at fixed H would instead modify the ground state at $N = -2$ and complicate a direct comparison. For large $\tilde{\mu}$ the evolution is nearly adiabatic: the state closely follows the instantaneous ground state into the deeper (true) vacuum, giving $P_{\text{false}} \approx 0$. For small $\tilde{\mu}$ the evolution becomes strongly non-adiabatic: the barrier *switches on* faster than the state can adjust, freezing population in an excited configuration so that the true vacuum is only weakly favored. As shown in Fig. 6(a), decreasing $\tilde{\mu}$ therefore increases P_{false} at late times for both Schrödinger and GKLS dynamics.

Figure 6(b) shows that in the adiabatic limit the state remains a pure ground state, with the rate of purity loss increasing as $\tilde{\mu}$ decreases. This is due to the larger Hubble rates in these runs non-

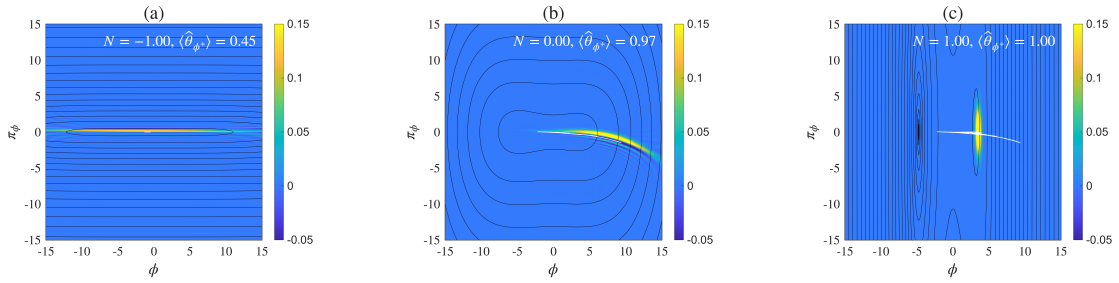


Figure 8: $\hat{L}_1 \propto \hat{\phi}$ & $\hat{L}_2 \propto \hat{\pi}_\phi$ SSE dynamics, Wigner functions for the combined SSE evolution (2.36), with columns corresponding to different snapshot times. Black curves are equal-energy contours of $K_S(N)$. Axes are ϕ and π_ϕ . In-panel text reports the e -fold N and the false-vacuum projector expectation value. The sonified video corresponding to these plots is available [via this link](#) with sonification method described in [69]. The white line corresponds to the prior evolution of the phase-space expectation values $\langle \hat{\phi} \rangle$ and $\langle \hat{\pi}_\phi \rangle$. The adiabaticity parameter used for this simulation is $\tilde{\mu} = 0.1$.

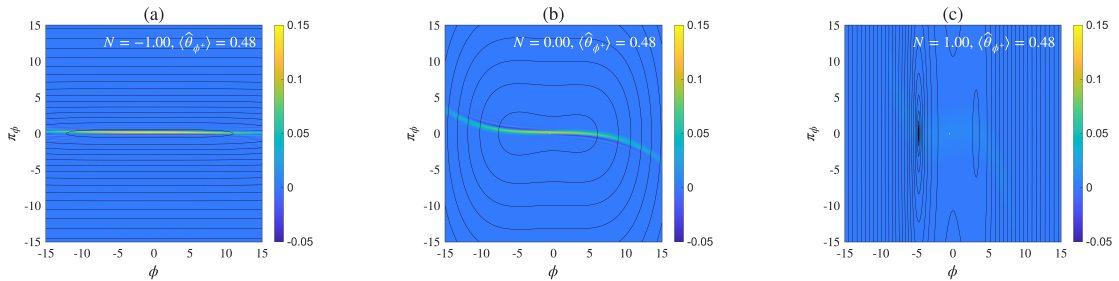


Figure 9: $\hat{L}_1 \propto \hat{\phi}$ & $\hat{L}_2 \propto \hat{\pi}_\phi$ GKLS dynamics, Wigner functions for Lindblad evolution with both channels active, with columns corresponding to different snapshot times. Black curves are equal-energy contours of $K_S(N)$. Axes are ϕ and π_ϕ . In-panel text reports the e -fold N and the false-vacuum projector expectation value. The sonified video corresponding to these plots is available [via this link](#) with sonification method described in [69]. The white line corresponds to the prior evolution of the phase-space expectation values $\langle \hat{\phi} \rangle$ and $\langle \hat{\pi}_\phi \rangle$. The adiabaticity parameter used for this simulation is $\tilde{\mu} = 0.1$.

adiabatically exciting higher states with subsequent decoherence diagonalizing the density operator. Turning on decoherence by increasing λ from 0 to 0.2 leaves $P_{\text{false}}(N)$ essentially unchanged but markedly increases the rate of purity loss; see Fig. 6(c).

Instantaneous ground state, Fig. 2: At $N = -2$ the state is a stretched Gaussian, effectively delocalized in ϕ when measured against the size of the barrier. By $N = 0$ the instantaneous ground state is approximately Gaussian and circular with comparable variances in ϕ and π_ϕ located in the basin of the true vacuum with $P_{\text{false}} \approx 0$. By $N = 1$ the state is strongly squeezed and localized at the true minimum.

Schrödinger equation, Fig. 3: The delocalized Wigner function non-adiabatically shears and develops interference fringes between the true and false vacua, while the purity remains 1. The state eventually freezes into a superposition over both vacua, with a false-vacuum occupation probability $P_{\text{false}} \approx 0.48$.

$\hat{L} \propto \hat{\phi}$ SSE trajectories, Fig. 4: The bath-induced dephasing channel acts as a continuous mea-

surement of ϕ . Each pure trajectory rapidly localizes into one well; fringes are suppressed and the Wigner function collapses to a highly squeezed and approximately Gaussian wavepacket. P_{false} drifts toward 0 or 1 depending on the selected well. The momentum expectation value can take large excursions due to a random walk in an almost flat π_ϕ direction.

$\hat{L} \propto \hat{\phi}$ GKLS dynamics, Fig. 5: The GKLS evolution produces a marginal in ϕ probability density that is very similar to that of the Schrödinger dynamics. However, bath-induced decoherence strongly suppresses nonclassical correlations (fringing and regions of Wigner-function negativity [72, 73]). By the end of the simulation interval, the Wigner function describes a highly mixed state with essentially the same false-vacuum occupation probability $P_{\text{false}} \approx 0.48$ as the closed-system dynamics.

Parameter sweeps, Fig. 6: Panel (a) shows that decreasing the adiabaticity parameter $\tilde{\mu}$ (at fixed initial state) increases late-time P_{false} for GKLS dynamics (2.26), reflecting non-adiabatic *barrier switch-on* that freezes population in an excited configuration. Panel (b) shows that purity loss accelerates as $\tilde{\mu}$ decreases, due to larger Hubble rates enhancing stochastic-inflation-induced mixing. We found that increasing λ at fixed $\tilde{\mu}$ leaves $P_{\text{false}}(N)$ essentially unchanged yet significantly speeds up purity loss as evidenced in Panel (c).

$\hat{L} \propto \hat{\pi}_\phi$ GKLS and stochastic-inflation SSE, Fig. 7: Panel (a) shows a purity sweep for the GKLS dynamics (2.33). With only the stochastic-inflation Lindblad operator present, increasing $\tilde{\mu}$ suppresses mixing and keeps the state closer to pure. Panels (b) and (c) display a representative SSE trajectory for the corresponding stochastic-inflation unraveling. The Wigner function undergoes strong shear and diffusion and is quite similar to the shape of the closed-system non-adiabatic dynamics in Fig. 3, but randomly translated, while in superposition over both vacua. Interestingly, since quantum signatures remain in the Wigner function, one finds a state that has *not* decohered, despite the fact that the purity has drastically decreased.

$\hat{L}_1 \propto \hat{\phi}, \hat{L}_2 \propto \hat{\pi}_\phi$ SSE dynamics, Fig. 8: The combined Itô SSE (2.36) implements simultaneous ϕ -dephasing and stochastic-inflation noise. Individual trajectories now experience both rapid well selection and diffusion in ϕ .

$\hat{L}_1 \propto \hat{\phi}, \hat{L}_2 \propto \hat{\pi}_\phi$ GKLS dynamics, Fig. 9: With both Lindblad channels active, the ensemble-averaged Wigner function becomes strongly mixed and approximately classical in both ϕ and π_ϕ . Relative to the $\hat{L} \propto \hat{\phi}$ case in Fig. 5, the additional $\hat{\pi}_\phi$ -channel accelerates phase-space diffusion and further suppresses residual nonclassical structures, providing a coarse-grained description of the combined bath and stochastic-inflation decoherence encoded in Eq. (2.34).

4 Late-time spectator dynamics with bath decoherence and stochastic inflation

In the previous section, we showed that non-adiabatic effects can significantly enhance the false-vacuum occupation of the light spectator-field zero mode during the transition from a kinetically-dominated to a potential-dominated epoch. The natural question is what happens afterwards, over the many e-folds that may still remain until the end of inflation. In this section, we argue that the combination of strong bath-induced decoherence, growing as $\propto e^{6N}$, and Hubble friction drives the spectator into the standard Starobinsky overdamped regime. In this limit the late-time false-vacuum decay is well described by an effective Arrhenius-type hopping rate [74] from the false vacuum F to the true vacuum

T . As discussed in §2.3, the coarse-grained spectator dynamics is governed by the normalised stochastic Schrödinger equation

$$\begin{aligned} d|\psi\rangle = -i \left(\frac{e^{-3N}}{2H\text{vol}} \hat{\pi}_\phi^2 + \frac{e^{3N}\text{vol}}{H} V(\hat{\phi}) \right) |\psi\rangle dN - \frac{H^2}{8\pi^2} \hat{\pi}_\phi^2 |\psi\rangle dN - \frac{iH}{2\pi} \hat{\pi}_\phi |\psi\rangle dW_2 \\ - \frac{131\pi\lambda^2 e^{6N}}{512\mu^5\text{vol}} (\hat{\phi} - \langle \hat{\phi} \rangle)^2 |\psi\rangle dN + \sqrt{\frac{131\pi\lambda^2 e^{6N}}{128\mu^5\text{vol}}} (\hat{\phi} - \langle \hat{\phi} \rangle) |\psi\rangle dW_1, \end{aligned} \quad (4.1)$$

where $dW_{1,2}$ are independent real Wiener increments. For large N , the potential term and strong λ -induced decoherence drive the state towards an approximate eigenstate of $\hat{\phi}$, so that the wavepacket becomes very sharply localized in $\hat{\phi}$,

$$\langle \hat{\phi}^2 \rangle - \langle \hat{\phi} \rangle^2 \approx 0. \quad (4.2)$$

We may drop the decoherence-induced noise terms proportional to the $\hat{\phi}$ deviation from the mean $(\hat{\phi} - \langle \hat{\phi} \rangle)$ recovering Eq. (2.30) and hence the stochastic expectation value equations (2.31) and (2.32). Due to localization in $\hat{\phi}$ we may replace $\langle V'(\hat{\phi}) \rangle \approx V'(\langle \hat{\phi} \rangle)$, and Eqs. (2.31) and (2.32) reduce to

$$d\langle \hat{\phi} \rangle = \frac{e^{-3N}}{\text{vol } H} \langle \hat{\pi}_\phi \rangle dN + \frac{H}{2\pi} dW, \quad (4.3)$$

$$d\langle \hat{\pi}_\phi \rangle = -\frac{\text{vol } e^{3N}}{H} V'(\langle \hat{\phi} \rangle) dN, \quad (4.4)$$

The associated delocalization in the $\hat{\pi}_\phi$ basis is not problematic here, because the Eq. (2.31) is linear in $\hat{\pi}_\phi$. When the field mass scale is sufficiently small compared to the Hubble scale, the dynamics is overdamped and the evolution of the expectation value is described by the one dimensional Langevin equation in N ,

$$d\langle \hat{\phi} \rangle = -\frac{V'(\langle \hat{\phi} \rangle)}{3H^2} dN + \frac{H}{2\pi} dW. \quad (4.5)$$

The standard Eyring–Kramers formula for overdamped escape in a multi-well potential [74] then yields the mean first-passage time from the false vacuum to the true vacuum,⁴

$$\langle N_{F \rightarrow T} \rangle \approx \frac{6\pi H^2}{\sqrt{V''(\phi_F) |V''(\phi_{\text{top}})|}} \exp \left\{ \frac{4\pi^2}{3H^4} [V(\phi_{\text{top}}) - V(\phi_F)] \right\}. \quad (4.6)$$

For the potential given in (1.3) the mean first-passage times are

$$\langle N_{F \rightarrow T} \rangle = \frac{3H^2\pi}{\mu^2} \sqrt{\frac{2(\beta_3 + \beta_4)}{\beta_4}} \exp \left[\frac{\pi^2(\beta_3 + 3\beta_4)\mu^4}{9(\beta_3 + \beta_4)^3 H^4} \right], \quad (4.7)$$

$$\langle N_{T \rightarrow F} \rangle = \frac{3H^2\pi}{\mu^2} \sqrt{\frac{2(\beta_4 - \beta_3)}{\beta_4}} \exp \left[\frac{\pi^2(\beta_3 - 3\beta_4)\mu^4}{9(\beta_3 - \beta_4)^3 H^4} \right]. \quad (4.8)$$

In this late-time, strongly localized limit the false-vacuum lifetime is therefore controlled by a single dimensionless parameter: the adiabaticity ratio μ/H , which fixes both the prefactor and, more importantly, the exponential sensitivity of the mean first-passage times in (4.8). Differentiating with

⁴This result coincides with stochastic tunneling first-passage-times as obtained in the classical limit of stochastic inflation, see eq. (4.6) of [5].

respect to $\tilde{\mu}$ we find a minimum mean first-passage time from the false to true vacuum at adiabaticity parameter

$$\tilde{\mu}_{\min} = \sqrt{\frac{3}{\pi}} \frac{(\beta_3 + \beta_4)^{3/4}}{(2\beta_3 + 6\beta_4)^{1/4}}. \quad (4.9)$$

For the parameters specified in (2.5), the minimum mean first-passage time is $\langle N_{\text{FPT}} \rangle_{\min} \approx 375$ e-folds, and no such hops are resolved within our simulation window. If inflation ends before a light field can relax via over-the-barrier hopping, our model suggests that quantum non-adiabatic effects may lead to greatly enhanced zero mode false-vacuum occupation probabilities at the end of inflation.

5 Summary

We have derived a Caldeira–Leggett–type open-system description for the zero mode of a spectator scalar field, together with a light-field stochastic inflation model in de Sitter space, in order to study the interplay between non-adiabatic dynamics and decoherence in an asymmetric double-well potential. This setup captures generic behavior that should also arise in realistic cosmological models but is often overlooked. A finite Hubble rate induces non-adiabatic evolution, exciting the instantaneous ground state and enhancing false-vacuum occupation, especially for light fields. Decoherence then reduces the purity until the state approaches a classical mixture of well-localized configurations in each potential well. The fastest purity decay occurs when the potential and kinetic contributions to the effective Hamiltonian are comparable, so that interference generated during the barrier switch-on is promptly decohered.

After decoherence, inter-well tunneling is strongly suppressed. Once off-diagonal elements in the field pointer basis are erased, sustained tunneling would require coherences that the Lindblad channel continually destroys. In our finite simulation window the false-vacuum occupation saturates with no drift under GKLS evolution, whereas small coherent oscillations persist in the closed system case. After the barrier switch-on the field is left in an excited state with enhanced false-vacuum occupation. As the system Hamiltonian transitions from a kinetically dominated to a potentially dominated regime, the underlying pure-state trajectories become increasingly localized, and any remaining transitions between wells are driven by diffusive stochastic-inflation kicks as UV modes cross into the IR. Over-the-barrier hops from the false to the true vacuum can in principle relax this excited state, but they are exponentially rare and must occur before the end of inflation; in the parameter ranges we explored, relaxation is inefficient and the zero mode typically exits inflation with non-adiabatically enhanced false-vacuum populations.

6 Data and code availability

Matlab and Mathematica codes to generate all figures and data in the paper can be found on GitHub: <https://github.com/rchristie95/CosmicLockdownMatlabAndMathematica>. Sonified videos of the Wigner function dynamics can be found on YouTube: <https://www.youtube.com/playlist?list=PLnFRudoWkGcH35xIe0bYtbGmptvwb7CH9> and sonification method is given in [69].

7 Acknowledgements

We thank Jason Pollack, Sarah Shandera and Varun Vaidya for helpful discussions. This work was supported by the Science and Technology Facilities Council (grant number ST/W001225/1). For the

purpose of open access, the authors have applied a Creative Commons Attribution (CC-BY) licence to any Author Accepted Manuscript version arising from this work. Supporting research data are available on reasonable request from the corresponding author, Robson Christie.

References

- [1] S.R. Coleman, *The Fate of the False Vacuum. 1. Semiclassical Theory*, *Phys. Rev. D* **15** (1977) 2929.
- [2] C.G. Callan, Jr. and S.R. Coleman, *The Fate of the False Vacuum. 2. First Quantum Corrections*, *Phys. Rev. D* **16** (1977) 1762.
- [3] S.R. Coleman and F. De Luccia, *Gravitational Effects on and of Vacuum Decay*, *Phys. Rev. D* **21** (1980) 3305.
- [4] S.W. Hawking and I.G. Moss, *Supercooled Phase Transitions in the Very Early Universe*, *Phys. Lett. B* **110** (1982) 35.
- [5] M. Noorbala, V. Vennin, H. Assadullahi, H. Firouzjahi and D. Wands, *Tunneling in Stochastic Inflation*, *JCAP* **09** (2018) 032 [[1806.09634](#)].
- [6] J.E. Camargo-Molina, M. Carrillo González and A. Rajantie, *Phase transitions in de sitter spacetimes: Quantum corrections*, *Physical Review D* **107** (2023) 063533.
- [7] G. Rigopoulos and A. Wilkins, *Computing first-passage times with the functional renormalisation group*, *Journal of Cosmology and Astroparticle Physics* **2023** (2023) 046.
- [8] T. Miyachi, J. Soda and J. Tokuda, *Stochastic tunneling in de sitter spacetime*, *Universe* **10** (2024) 292.
- [9] M. Sher, *Electroweak Higgs Potentials and Vacuum Stability*, *Phys. Rept.* **179** (1989) 273.
- [10] G. Isidori, G. Ridolfi and A. Strumia, *On the metastability of the standard model vacuum*, *Nucl. Phys. B* **609** (2001) 387 [[hep-ph/0104016](#)].
- [11] G. Degrassi, S. Di Vita, J. Elias-Miro, J.R. Espinosa, G.F. Giudice, G. Isidori et al., *Higgs mass and vacuum stability in the Standard Model at NNLO*, *JHEP* **08** (2012) 098 [[1205.6497](#)].
- [12] D. Buttazzo, G. Degrassi, P.P. Giardino, G.F. Giudice, F. Sala, A. Salvio et al., *Investigating the near-criticality of the Higgs boson*, *JHEP* **12** (2013) 089 [[1307.3536](#)].
- [13] A. Andreassen, W. Frost and M.D. Schwartz, *Consistent Use of the Standard Model Effective Potential*, *Phys. Rev. Lett.* **113** (2014) 241801 [[1408.0292](#)].
- [14] J.R. Espinosa, G.F. Giudice and A. Riotto, *Cosmological implications of the Higgs mass measurement*, *JCAP* **05** (2008) 002 [[0710.2484](#)].
- [15] S. Chigusa, T. Moroi and Y. Shoji, *Decay Rate of Electroweak Vacuum in the Standard Model and Beyond*, *Phys. Rev. D* **97** (2018) 116012 [[1803.03902](#)].
- [16] T. Markkanen, A. Rajantie and S. Stopyra, *Cosmological Aspects of Higgs Vacuum Metastability*, *Front. Astron. Space Sci.* **5** (2018) 40 [[1809.06923](#)].
- [17] V. Branchina and E. Messina, *Stability, Higgs Boson Mass and New Physics*, *Phys. Rev. Lett.* **111** (2013) 241801 [[1307.5193](#)].
- [18] W.M. Itano, D.J. Heinzen, J.J. Bollinger and D.J. Wineland, *Quantum zeno effect*, *Physical Review A* **41** (1990) 2295.
- [19] W. Li, N. Es' haqi Sani, W.-Z. Zhang and D. Vitali, *Quantum zeno effect in self-sustaining systems: Suppressing phase diffusion via repeated measurements*, *Physical Review A* **103** (2021) 043715.

[20] M. Sakagami, *Evolution From Pure States Into Mixed States in De Sitter Space*, *Prog. Theor. Phys.* **79** (1988) 442.

[21] R.H. Brandenberger, R. Laflamme and M. Mijic, *Classical Perturbations From Decoherence of Quantum Fluctuations in the Inflationary Universe*, *Mod. Phys. Lett. A* **5** (1990) 2311.

[22] A. Matacz, *The Emergence of classical behavior in the quantum fluctuations of a scalar field in an expanding universe*, *Class. Quant. Grav.* **10** (1993) 509.

[23] F. Lombardo and F.D. Mazzitelli, *Coarse graining and decoherence in quantum field theory*, *Phys. Rev. D* **53** (1996) 2001 [[hep-th/9508052](#)].

[24] E. Calzetta and B.L. Hu, *Quantum fluctuations, decoherence of the mean field, and structure formation in the early universe*, *Phys. Rev. D* **52** (1995) 6770 [[gr-qc/9505046](#)].

[25] D. Polarski and A.A. Starobinsky, *Semiclassicality and decoherence of cosmological perturbations*, *Class. Quant. Grav.* **13** (1996) 377 [[gr-qc/9504030](#)].

[26] C. Kiefer, D. Polarski and A.A. Starobinsky, *Quantum to classical transition for fluctuations in the early universe*, *Int. J. Mod. Phys. D* **07** (1998) 455 [[gr-qc/9802003](#)].

[27] F.C. Lombardo and D. Lopez Nacir, *Decoherence during inflation: The Generation of classical inhomogeneities*, *Phys. Rev. D* **72** (2005) 063506 [[gr-qc/0506051](#)].

[28] C. Burgess, R. Holman and D. Hoover, *Decoherence of inflationary primordial fluctuations*, *Phys. Rev. D* **77** (2008) 063534 [[astro-ph/0601646](#)].

[29] T. Prokopec and G.I. Rigopoulos, *Decoherence from Isocurvature perturbations in Inflation*, *JCAP* **0711** (2007) 029 [[astro-ph/0612067](#)].

[30] J.W. Sharman and G.D. Moore, *Decoherence due to the Horizon after Inflation*, *JCAP* **0711** (2007) 020 [[0708.3353](#)].

[31] C. Kiefer and D. Polarski, *Why do cosmological perturbations look classical to us?*, *Adv. Sci. Lett.* **2** (2009) 164 [[0810.0087](#)].

[32] C. Kiefer, F. Queisser and A.A. Starobinsky, *Cosmological Constant from Decoherence*, *Class. Quant. Grav.* **28** (2011) 125022 [[1010.5331](#)].

[33] T.C. Bachlechner, *Decoherence delays false vacuum decay*, *Class. Quant. Grav.* **30** (2013) 095012 [[1203.1619](#)].

[34] M. Franco and E. Calzetta, *Decoherence in the cosmic background radiation*, *Class. Quant. Grav.* **28** (2011) 145024 [[1103.0188](#)].

[35] C.P. Burgess, R. Holman, G. Tasinato and M. Williams, *EFT Beyond the Horizon: Stochastic Inflation and How Primordial Quantum Fluctuations Go Classical*, *JHEP* **03** (2015) 090 [[1408.5002](#)].

[36] E. Nelson, *Quantum Decoherence During Inflation from Gravitational Nonlinearities*, *JCAP* **1603** (2016) 022 [[1601.03734](#)].

[37] K.K. Boddy, S.M. Carroll and J. Pollack, *How decoherence affects the probability of slow-roll eternal inflation*, *Physical Review D* **96** (2017) 023539.

[38] N. Bao, A. Chatwin-Davies, J. Pollack and G.N. Remmen, *Cosmological Decoherence from Thermal Gravitons*, *JHEP* **08** (2020) 065 [[1911.10207](#)].

[39] S. Brahma, O. Alaryani and R. Brandenberger, *Entanglement entropy of cosmological perturbations*, *Phys. Rev. D* **102** (2020) 043529 [[2005.09688](#)].

[40] T. Colas, J. Grain and V. Vennin, *Benchmarking the cosmological master equations*, *Eur. Phys. J. C* **82** (2022) 1085 [[2209.01929](#)].

[41] C.P. Burgess, R. Holman, G. Kaplanek, J. Martin and V. Vennin, *Minimal decoherence from inflation*, *JCAP* **07** (2023) 022 [[2211.11046](#)].

[42] A. Daddi Hammou and N. Bartolo, *Cosmic decoherence: primordial power spectra and non-Gaussianities*, *JCAP* **04** (2023) 055 [[2211.07598](#)].

[43] T. Colas, J. Grain and V. Vennin, *Quantum recoherence in the early universe*, *EPL* **142** (2023) 69002 [[2212.09486](#)].

[44] C.M. Sou, D.H. Tran and Y. Wang, *Decoherence of cosmological perturbations from boundary terms and the non-classicality of gravity*, *JHEP* **04** (2023) 092 [[2207.04435](#)].

[45] K. Boutivas, D. Katsinis, G. Pastras and N. Tetradis, *Entanglement in cosmology*, *JCAP* **04** (2024) 017 [[2310.17208](#)].

[46] T. Colas, C. de Rham and G. Kaplanek, *Decoherence out of fire: purity loss in expanding and contracting universes*, *JCAP* **05** (2024) 025 [[2401.02832](#)].

[47] T. Colas, J. Grain, G. Kaplanek and V. Vennin, *In-in formalism for the entropy of quantum fields in curved spacetimes*, *JCAP* **08** (2024) 047 [[2406.17856](#)].

[48] J. de Kruijf and N. Bartolo, *The effect of quantum decoherence on inflationary gravitational waves*, *JCAP* **11** (2024) 041 [[2408.02563](#)].

[49] C.P. Burgess, T. Colas, R. Holman, G. Kaplanek and V. Vennin, *Cosmic purity lost: perturbative and resummed late-time inflationary decoherence*, *JCAP* **08** (2024) 042 [[2403.12240](#)].

[50] C.P. Burgess, R. Holman and G. Kaplanek, *Inflationary Decoherence from the Gravitational Floor*, [2509.07769](#).

[51] S. Cespedes, S. de Alwis and F. Quevedo, *Cosmology, Decoherence and the Second Law*, [2509.07077](#).

[52] J. de Kruijf, G. Galloni and N. Bartolo, *The first data-driven bounds on the quantum decoherence of inflationary gravitational waves*, [2511.14727](#).

[53] F. Sano and J. Tokuda, *False and genuine decoherence in the early universe: a local observer and time-averaged observables*, *JHEP* **07** (2025) 266 [[2504.10472](#)].

[54] F. Lopez and N. Bartolo, *Quantum signatures and decoherence during inflation from deep subhorizon perturbations*, [2503.23150](#).

[55] H. Takeda and T. Tanaka, *Quantum decoherence of gravitational waves*, *Phys. Rev. D* **111** (2025) 104080 [[2502.18560](#)].

[56] G. Lindblad, *On the generators of quantum dynamical semigroups*, *Communications in Mathematical Physics* **48** (1976) 119.

[57] V. Gorini, A. Kossakowski and E.C.G. Sudarshan, *Completely positive dynamical semigroups of N-level systems*, *Journal of Mathematical Physics* **17** (1976) 821.

[58] V.P. Belavkin, *Nondemolition measurements, nonlinear filtering and dynamic programming of quantum stochastic processes*, in *Modeling and Control of Systems*, pp. 245–265, Springer (1989).

[59] I. Percival, *Quantum state diffusion*, Cambridge University Press (1998).

[60] H.-P. Breuer and F. Petruccione, *The theory of open quantum systems*, Oxford University Press on Demand (2002).

[61] A.O. Caldeira and A.J. Leggett, *Path integral approach to quantum brownian motion*, *Physica A: Statistical mechanics and its Applications* **121** (1983) 587.

[62] A.A. Starobinsky, *Stochastic de Sitter (inflationary) stage in the early Universe*, *Lect. Notes Phys.* **246** (1986) 107.

[63] Y. Nambu and M. Sasaki, *Stochastic Stage of an Inflationary Universe Model*, *Phys. Lett. B* **205** (1988) 441.

[64] A.A. Starobinsky and J. Yokoyama, *Equilibrium state of a self-interacting scalar field in the De Sitter background*, *Phys. Rev. D* **50** (1994) 6357.

[65] F. Finelli, G. Marozzi, A.A. Starobinsky, G. Vacca and G. Venturi, *Generation of fluctuations during inflation: Comparison of stochastic and field-theoretic approaches*, *Phys. Rev. D* **79** (2009) 044007.

[66] V. Vennin and D. Wands, *Quantum Diffusion and Large Primordial Perturbations from Inflation*, in *Primordial Black Holes*, p. 201–227, Springer Nature Singapore (2025), DOI [\[2402.12672\]](https://doi.org/10.1007/978-981-16-2126-7_10).

[67] Z. Haba, *Stochastic inflation with quantum and thermal noise*, *The European Physical Journal C* **78** (2018) 596.

[68] Z. Haba, *Stabilization of starobinsky–vilenkin stochastic inflation by an environmental noise*, *International Journal of Modern Physics D* **28** (2019) 1950085.

[69] R. Christie and J. Trayford, *The sound of decoherence*, *arXiv preprint arXiv:2412.17045* (2024) .

[70] E. Wigner, *On the quantum correction for thermodynamic equilibrium*, *Physical review* **40** (1932) 749.

[71] A. Royer, *Wigner function in liouville space: a canonical formalism*, *Physical Review A* **43** (1991) 44.

[72] R.L. Hudson, *When is the Wigner quasi-probability density non-negative?*, *Reports on Mathematical Physics* **6** (1974) 249.

[73] A. Kenfack and K. Życzkowski, *Negativity of the Wigner function as an indicator of non-classicality*, *Journal of Optics B: Quantum and Semiclassical Optics* **6** (2004) 396.

[74] D. Chandler, *Introduction to modern statistical mechanics*, Oxford University Press (1987).

[75] C.W. Misner, *A minisuperspace example: the gowdy t 3 cosmology*, *Physical Review D* **8** (1973) 3271.

[76] C. Kiefer and B. Sandhöfer, *Quantum cosmology*, *Zeitschrift für Naturforschung A* **77** (2022) 543.

[77] G.A. Pavliotis, *Stochastic processes and applications*, *Texts in Applied Mathematics* **60** (2014) .

[78] D. Comparat, *General conditions for quantum adiabatic evolution*, *Physical Review A—Atomic, Molecular, and Optical Physics* **80** (2009) 012106.

[79] L. Diósi, N. Gisin and W.T. Strunz, *Non-markovian quantum state diffusion*, *Physical Review A* **58** (1998) 1699.

[80] L. Diósi and L. Feráldi, *General non-markovian structure of gaussian master and stochastic schrödinger equations*, *Physical review letters* **113** (2014) 200403.

A Master equations and bath correlators in de Sitter

This appendix derives the time-local Gorini-Kossakowski-Lindblad-Sudarshan (GKLS) equation governing the infrared dynamics of a light scalar test field in de Sitter space. Throughout, we restrict attention to the *homogeneous zero-mode* ($k = 0$) of each field, neglecting all spatially varying ($k \neq 0$) modes. After this truncation, the fields depend only on the number of e -folds $N \equiv \ln a$, and we omit explicit zero-mode subscripts for brevity.

A.1 Single-oscillator bath in de Sitter

We begin with the four-dimensional action

$$S = - \int d^4x \sqrt{-g} \left(\mathcal{L}_\phi + \mathcal{L}_\chi - \mathcal{L}_{\text{int}}^{(k)} \right) \quad (\text{A.1})$$

with the system and environment Lagrangian densities

$$\mathcal{L}_\phi = \frac{1}{2}(\partial\phi)^2 - V(\phi) \quad \text{and} \quad \mathcal{L}_\chi = \frac{1}{2}(\partial\chi)^2 - \frac{m^2}{2}\chi^2, \quad (\text{A.2})$$

and system potential given in eq. (1.3). We consider various four point interactions

$$\mathcal{L}_{\text{int}}^{(1)} = \underline{\lambda}_1 \phi^3 \chi, \quad \mathcal{L}_{\text{int}}^{(2)} = \underline{\lambda}_2 \phi^2 \chi^2, \quad \mathcal{L}_{\text{int}}^{(3)} = \underline{\lambda}_3 \phi \chi^3 \quad (\text{A.3})$$

where $\underline{\lambda}_i$ are bare (denoted by the under bar) dimensionless coupling strengths. To isolate the long-wavelength (infrared) dynamics relevant for stochastic and open-system treatments, we discard all spatial gradients and retain only the homogeneous contributions,

$$\phi(x, N) \rightarrow \phi(N), \quad \chi(x, N) \rightarrow \chi(N). \quad (\text{A.4})$$

This restriction removes all higher-momentum modes and yields a Lagrangian density describing two coupled oscillators evolving in de Sitter [75, 76],

$$\mathcal{L}(t) = a^3(t) \left[\frac{\dot{\phi}^2}{2} - V(\phi) + \frac{\dot{\chi}^2}{2} - \frac{m^2}{2}\chi^2 - \mathcal{L}_{\text{int}}^{(k)} \right]. \quad (\text{A.5})$$

To pass to Hamiltonian language we define canonical momenta in the usual way,

$$\pi_\phi \equiv \frac{\partial \mathcal{L}}{\partial \dot{\phi}} = a^3 \dot{\phi}, \quad \pi_\chi \equiv \frac{\partial \mathcal{L}}{\partial \dot{\chi}} = a^3 \dot{\chi}, \quad (\text{A.6})$$

and after a brief calculation obtain the Hamiltonian function

$$\mathcal{H} = a^3(t) \left[\frac{\dot{\phi}^2}{2} + V(\phi) + \frac{\dot{\chi}^2}{2} + \frac{m^2}{2}\chi^2 + \mathcal{L}_{\text{int}}^{(k)} \right]. \quad (\text{A.7})$$

For simulations N is more convenient than cosmic time t , $a(t) = e^{Ht} = e^N$ and therefore $\dot{\phi} = H\phi'$. In terms of N the canonical momenta become

$$\pi_\phi = e^{3N} H\phi', \quad \pi_\chi = e^{3N} H\chi', \quad (\text{A.8})$$

and the zero-mode Hamiltonian operator reads

$$\hat{K}(N) = \frac{e^{-3N}}{2H\text{vol}} \hat{\pi}_\phi^2 + \frac{e^{3N}\text{vol}}{H} V(\hat{\phi}) + \frac{e^{-3N}}{2H\text{vol}} \hat{\pi}_\chi^2 + \frac{m_\chi^2 \text{vol} e^{3N}}{2H} \hat{\chi}^2 + \frac{\text{vol} e^{3N}}{H} \mathcal{L}_{\text{int}}^{(k)}. \quad (\text{A.9})$$

We can diagonalise the bath Hamiltonian which leads to the compact expression for the bath χ oscillator Hamiltonian

$$\hat{K}_B^{(\chi)}(N) = \omega_\chi \left(\hat{b}^\dagger(N) \hat{b}(N) + \frac{1}{2} \right), \quad \text{with} \quad \omega_\chi \equiv \frac{m_\chi}{H} \quad \text{and} \quad \hat{b}(N) = \sqrt{\frac{m_\chi \text{vol} e^{3N}}{2}} \chi + \frac{i}{\sqrt{2m_\chi \text{vol} e^{3N}}} \hat{\pi}_\chi. \quad (\text{A.10})$$

If we assume that the system and bath are coupled at $N = N_0$ we can write down a Nakajima-Zwanzig equation [60] in the interaction picture (operators acquire a subscript I) with the reduced density matrix of the ϕ field obeying

$$\dot{\rho}_I(N) = -\underline{\lambda}_k^2 \int_{N_0}^N d\bar{N} C_k(N, \bar{N}) [\hat{S}_I^{(k)}(N), [\hat{S}_I^{(k)}(\bar{N}), \rho_I]]. \quad (\text{A.11})$$

We have split the interaction term $\hat{S}_I^{(k)} \otimes \hat{B}_I^{(k)}$ as

$$\hat{S}_I^{(k)}(N) = \frac{\text{vol} e^{3N}}{H} \hat{\phi}_I^{4-k}(N), \quad \text{and} \quad \hat{B}_I^{(k)}(N) = \lambda \hat{\chi}_I^k(N) \quad (\text{A.12})$$

and the bath enters only through the fluctuation correlation functions:

$$C_k(N, \bar{N}) = \langle \mathbf{0}_{N_0} | \hat{\chi}_I^k(N) \hat{\chi}_I^k(\bar{N}) | \mathbf{0}_{N_0} \rangle - \langle \mathbf{0}_{N_0} | \hat{\chi}_I^k(N) | \mathbf{0}_{N_0} \rangle \langle \mathbf{0}_{N_0} | \hat{\chi}_I^k(\bar{N}) | \mathbf{0}_{N_0} \rangle. \quad (\text{A.13})$$

As the χ field evolves under a quadratic Hamiltonian we may use Isserlis theorem [77] to write the higher fluctuation correlation functions in terms of the two-point function C_1 as

$$C_2(N, \bar{N}) = 2C_1(N, \bar{N})^2 \quad \text{and} \quad C_3(N, \bar{N}) = 9C_1(N, N)C_1(\bar{N}, \bar{N})C_1(N, \bar{N}) + 6C_1(N, \bar{N})^3. \quad (\text{A.14})$$

To evaluate this two-point function we start by expressing the interaction picture χ operator in terms of ladder operators as

$$\hat{\chi}_I(N) = \frac{e^{-\frac{3}{2}N}}{\sqrt{2\omega_\chi H \text{vol}}} \left[\hat{b}(N) e^{-i\omega_\chi \Delta} + \hat{b}^\dagger(N) e^{i\omega_\chi \Delta} \right] \quad (\text{A.15})$$

where we introduce the time differences $\Delta = N - N_0$ and $\bar{\Delta} = \bar{N} - N_0$ for brevity. We can write the interaction picture field operator in terms of ladder operators at N_0 as

$$\begin{aligned} \hat{\chi}_I(N) = \frac{e^{-\frac{3}{2}N}}{\sqrt{2\omega_\chi H \text{vol}}} & \left\{ \left[\cosh\left(\frac{3\Delta}{2}\right) \hat{b}(N_0) + \sinh\left(\frac{3\Delta}{2}\right) \hat{b}^\dagger(N_0) \right] e^{-i\omega_\chi \Delta} \right. \\ & \left. + \left[\cosh\left(\frac{3\Delta}{2}\right) \hat{b}^\dagger(N_0) + \sinh\left(\frac{3\Delta}{2}\right) \hat{b}(N_0) \right] e^{i\omega_\chi \Delta} \right\} \quad (\text{A.16}) \end{aligned}$$

by making use of the commutation relations

$$[b(N), b^\dagger(N_0)] = \cosh\left(\frac{3}{2}\Delta\right), \quad [b(N), b(N_0)] = -\sinh\left(\frac{3}{2}\Delta\right), \quad [b^\dagger(N), b^\dagger(N_0)] = \sinh\left(\frac{3}{2}\Delta\right). \quad (\text{A.17})$$

The two point function is thus given by

$$\begin{aligned} C_1(N, \bar{N}) = \frac{e^{-\frac{3}{2}(N+\bar{N})}}{2H\omega_\chi \text{vol}} & \left\{ \cosh\left[\frac{1}{2}\Delta(3 + 2i\omega_\chi)\right] + \sinh\left[\frac{1}{2}\Delta(3 - 2i\omega_\chi)\right] \right\} \\ & \left\{ \cosh\left[\frac{1}{2}\bar{\Delta}(3 - 2i\omega_\chi)\right] + \sinh\left[\frac{1}{2}\bar{\Delta}(3 + 2i\omega_\chi)\right] \right\} \quad (\text{A.18}) \end{aligned}$$

with higher correlators C_2 and C_3 given by eq. (A.14).

A.2 Continuous oscillator bath spectra

To include a continuum of heavy modes we replace the single oscillator χ with a set $\{\chi_m\}$ labelled by their mass m . The bulk Lagrangian is therefore generalised to

$$L(t) = \text{vol} \cdot a^3 \left[\frac{1}{2} \dot{\phi}^2 - V(\phi) - \frac{1}{\mu} \int_0^\infty dm \left(\frac{1}{2} \dot{\chi}_m^2 - \frac{1}{2} m^2 \chi_m^2 + \Delta_k g^{k/2}(m) \phi^{4-k} \chi_m^k \right) \right] \quad \text{with} \quad g(m) = \frac{m}{\mu} e^{-m/\Lambda}. \quad (\text{A.19})$$

The form of the spectral density $g(m)$ is introduced to compensate the mass scaling of the correlators, $C_k(N, \bar{N}; m) \propto m^{-k}$, so that the integrand in (A.19) results in Markovian white noise rather than power-law suppressed coloured noise. Λ is a high mass cutoff which acts as a regulator as we later take $\Lambda \rightarrow \infty$. In the remainder of this appendix we derive renormalised Markovian master equations corresponding to the three \mathcal{L} choices.

$\phi^3 \chi$ interaction:

The continuous two point correlation function is thus

$$C_1^{\text{cont}}(N, \bar{N}, \Lambda) = \frac{1}{\mu^2} \int_0^\infty dm \int_0^\infty dm' \sqrt{g(m)g(m')} \langle \mathbf{0}_{N_0} | \chi_{m,I}(N) \chi_{m',I}(\bar{N}) | \mathbf{0}_{N_0} \rangle. \quad (\text{A.20})$$

As the environmental fields of different masses are uncorrelated, $\langle \chi_{m,I}(N) \chi_{m',I}(\bar{N}) \rangle \propto \delta(m - m') C_1(N, \bar{N}; m)$, so the double integral reduces to a single mass integral:

$$C_1^{\text{cont}}(N, \bar{N}, \Lambda) = \frac{1}{\mu^2} \int_0^\infty dm g(m) C_1(N, \bar{N}; m). \quad (\text{A.21})$$

Performing this integral yields

$$C_1^{\text{cont}}(N, \bar{N}, \Lambda) = -\frac{i H \Lambda}{2\mu^3 \text{vol}} e^{-\frac{3}{2}(N+\bar{N})} \left[\begin{aligned} & \sinh\left(\frac{3}{2}(N - N_0)\right) \left(-\frac{H \cosh\left(\frac{3}{2}(N_0 - \bar{N})\right)}{iH + (N - 2N_0 + \bar{N})\Lambda} + \frac{H \sinh\left(\frac{3}{2}(N_0 - \bar{N})\right)}{iH + (N - \bar{N})\Lambda} \right) \\ & + H \cosh\left(\frac{3}{2}(N - N_0)\right) \left(\frac{\cosh\left(\frac{3}{2}(N_0 - \bar{N})\right)}{-iH + (N - \bar{N})\Lambda} - \frac{i \sinh\left(\frac{3}{2}(N_0 - \bar{N})\right)}{H + i(N - 2N_0 + \bar{N})\Lambda} \right) \end{aligned} \right]. \quad (\text{A.22})$$

When passing from these non-local kernels to Markovian ones we let $\Lambda \rightarrow \infty$ and apply the Sokhotski-Plemelj formula

$$\frac{\Lambda}{(i \pm \Lambda \alpha)} \xrightarrow{\Lambda \rightarrow \infty} i\pi\delta(\alpha) \mp \mathcal{PV} \left(\frac{1}{\alpha} \right) \quad \text{with} \quad \int_0^\infty \mathcal{PV} \left(\frac{f(x)}{x} \right) dx = \int_0^\infty \frac{f(x) - f(0)}{x} dx. \quad (\text{A.23})$$

After discarding the poles on the zero-measure surface $N + \bar{N} = 2N_0$ we arrive at the decomposition

$$\text{Re}[C_1^{\text{cont}}(N, \bar{N}, \Lambda \rightarrow \infty)] = \frac{\pi H^2}{2\mu^3 \text{vol}} e^{-3N} \cosh[3(N - N_0)] \delta(N - \bar{N}), \quad (\text{A.24a})$$

$$\text{Im}[C_1^{\text{cont}}(N, \bar{N}, \Lambda \rightarrow \infty)] = -\frac{H^2 e^{-3(N+\bar{N})} \left[e^{3\bar{N}}(N - N_0) + e^{3N}(\bar{N} - N_0) \right]}{2(N - 2N_0 + \bar{N}) \mu^3 \text{vol}} \mathcal{PV} \left(\frac{1}{N - \bar{N}} \right). \quad (\text{A.24b})$$

The first line is an ultralocal white-noise spike; the second is purely imaginary, antisymmetric, and appears as a principal value term. While the imaginary part is finite, the real part grows without bound as the interaction switch-on time is taken to the infinite past $N_0 \rightarrow -\infty$, due to infinite de Sitter squeezing. To obtain a finite late-time generator we introduce the renormalized coupling

$$\lambda_1^2 \equiv \lim_{N_0 \rightarrow -\infty} \underline{\lambda}_1^2 e^{-3N_0}, \quad \text{so that} \quad \underline{\lambda}_1^2 = \lambda_1^2 e^{3N_0}. \quad (\text{A.25})$$

The real δ spike dominates the principal value pole which tends to zero with this renormalization scheme. We therefore retain only the symmetric real kernel $\text{Re}[C_1^{\text{cont}}(N, \bar{N}, \Lambda \rightarrow \infty)]$ when performing the integral in eq. (A.18), which yields a completely positive GKLS semigroup with pure dephasing of the form

$$\partial_N \rho = -i[\hat{K}_S(N), \rho] - \frac{\pi \lambda_1^2 \text{vol} e^{6N}}{8\mu^3} [\hat{\phi}^3, [\hat{\phi}^3, \hat{\rho}]], \quad (\text{A.26})$$

with system Hamiltonian given in eq. (2.3). Note the dephasing term picks up an additional factor of $1/2$ in since we only integrate \bar{N} over half of the $\delta(N - \bar{N})$ function. In the position basis (field value space) this dissipator acts as $\partial_N \rho(\phi, \phi'; N)|_{\text{diss}} = \frac{\lambda_1^2 \text{vol} e^{6N}}{8\mu^3} (\phi^3 - \phi'^3)^2 \rho(\phi, \phi'; N)$, so it leaves the position marginal $\rho(\phi, \phi; N)$ unchanged but strongly suppresses off-diagonal coherences for $\phi \neq \phi'$.

$\phi^2 \chi^2$ interaction:

Following eq. (A.14) and similar steps to the two point derivation we have

$$C_2^{\text{cont}}(N, \bar{N}, \Lambda) = \frac{2}{\mu^2} \int_0^\infty dm g^2(m) C_1(N, \bar{N}; m)^2. \quad (\text{A.27})$$

Performing this integral yields

$$\begin{aligned} C_2^{\text{cont}}(N, \bar{N}, \Lambda) = & \frac{e^{-3(N+\bar{N})} H \Lambda}{4\mu^4 \text{vol}^2} \left[\frac{H \cosh^2(\frac{3}{2}(\bar{N} - N_0)) \sinh(3N - 3N_0)}{H - i(\bar{N} - N_0)\Lambda} \right. \\ & + \frac{H \cosh^2(\frac{3}{2}(\bar{N} - N_0)) \sinh^2(\frac{3}{2}(N - N_0))}{H - i(N - 2N_0 + \bar{N})\Lambda} + \frac{H \sinh^2(\frac{3}{2}(N - N_0)) \sinh(3(\bar{N} - N_0))}{H - i(N - N_0)\Lambda} \\ & + \frac{H \sinh(3N - 3N_0) \sinh^2(\frac{3}{2}(N_0 - \bar{N}))}{H - i(N_0 - \bar{N})\Lambda} + \frac{H \sinh^2(\frac{3}{2}(N - N_0)) \sinh^2(\frac{3}{2}(\bar{N} - N_0))}{H - i(N - \bar{N})\Lambda} \\ & - i \cosh^2(\frac{3}{2}(N - N_0)) \left(\frac{H \cosh^2(\frac{3}{2}(\bar{N} - N_0))}{-iH + (N - \bar{N})\Lambda} - \frac{H \sinh(3(\bar{N} - N_0))}{iH - (N - N_0)\Lambda} + \frac{H \sinh^2(\frac{3}{2}(\bar{N} - N_0))}{-iH + (N - 2N_0 + \bar{N})\Lambda} \right) \\ & \left. + \sinh(3N - 3N_0) \sinh(3(\bar{N} - N_0)) \right]. \quad (\text{A.28}) \end{aligned}$$

We can apply the Sokhotski-Plemelj formula eq. (A.23) to all terms except the final term $\propto \Lambda e^{-\frac{3}{2}(N+\bar{N})} \sinh(3N - 3N_0) \sinh(3(\bar{N} - N_0))$ in C_2^{cont} which is infinite in the $\Lambda \rightarrow \infty$ limit and analogous to a loop divergence in QFT. This term is removed by redefining the quartic coupling λ_2 with a counter term. The poles of the Sokhotski-Plemelj formula eq. (A.23) are

$$\alpha_1 = N - \bar{N}, \quad \alpha_2 = N - 2N_0 + \bar{N}, \quad \alpha_3 = N - N_0, \quad \text{and} \quad \alpha_4 = \bar{N} - N_0. \quad (\text{A.29})$$

Considering eq. (A.11) the poles α_2 and α_3 correspond to equivalent zero-measure integrals $N = \bar{N} = N_0$ and α_4 is an initial bath contact term $\bar{N} = N_0$. α_1 is the relevant pole for a Markovian master

equation and after discarding irrelevant poles we obtain

$$\text{Re}(C_4^{\text{ohm}}(N, \bar{N}, \Lambda \rightarrow \infty)) = \frac{\pi H^2}{4\mu^4 \text{vol}^2} e^{-6N} \cosh[3(N - N_0)] \delta(N - \bar{N}), \quad (\text{A.30})$$

$$\begin{aligned} \text{Im}(C_4^{\text{ohm}}(N, \bar{N}, \Lambda \rightarrow \infty)) &= \frac{e^{-3(N+\bar{N})} H^2}{4(N - N_0)(N - 2N_0 + \bar{N})(\bar{N} - N_0) \mu^4 \text{vol}^2} \mathcal{PV} \left(\frac{1}{N - \bar{N}} \right) \\ &\times \left\{ -(N - N_0)(N_0 - \bar{N})^2 \cosh[3(N - N_0)] + (N - N_0)^2 (N_0 - \bar{N}) \cosh[3(N_0 - \bar{N})] \right. \\ &\left. + (N - \bar{N})(N - 2N_0 + \bar{N}) \left[(N - N_0) \sinh[3(N - N_0)] + (\bar{N} - N_0) \sinh[3(N_0 - \bar{N})] \right] \right\}. \quad (\text{A.31}) \end{aligned}$$

both these expressions grow without bound as $N_0 \rightarrow -\infty$ due to exponential de Sitter squeezing. The real part diverges as e^{-6N_0} and the imaginary part as e^{-3N_0} . To obtain a finite late-time generator we introduce the renormalized coupling

$$\lambda_2^2 \equiv \lim_{N_0 \rightarrow -\infty} \underline{\lambda}_2^2 e^{-6N_0}, \quad \text{so that} \quad \underline{\lambda}_2^2 = \lambda_2^2 e^{6N_0}. \quad (\text{A.32})$$

with this renormalization the imaginary part tends to zero and we derive the master equation

$$\partial_N \rho = -i [\hat{K}_S(N), \rho] - \frac{\pi \lambda_2^2 e^{6N}}{64\mu^4} [\hat{\phi}^2, [\hat{\phi}^2, \hat{\rho}]], \quad (\text{A.33})$$

with system Hamiltonian given in eq. (2.3). In the position basis the above dissipator is diagonal in ϕ^2 , so it suppresses coherences between configurations with different values of ϕ^2 but leaves intact superpositions related by the \mathbb{Z}_2 symmetry $\phi \rightarrow -\phi$. Consequently, it does not collapse a double-well superposition $|+\phi_0\rangle \pm |-\phi_0\rangle$ into a single well, since $(+\phi_0)^2 = (-\phi_0)^2$.

$\phi\chi^3$ interaction:

Following eq. (A.14) and similar steps to the two point derivation we have

$$C_3^{\text{cont}}(N, \bar{N}, \Lambda) = \frac{1}{\mu^2} \int_0^\infty dm g^3(m) [9C_1(N, \bar{N}; m)C_1(N, N; m)C_1(\bar{N}, \bar{N}; m) + 6C_1(N, \bar{N}; m)^3]. \quad (\text{A.34})$$

The integrated expressions are lengthy and provided in the supplementary Mathematica notebook. We follow similar procedure to the C_2^{cont} (although loop divergences do not appear in this case) to obtain

$$\begin{aligned} \text{Re}(C_3^{\text{ohm}}(N, \bar{N}, \Lambda \rightarrow \infty)) &= \frac{e^{-9N} H^2 \pi}{128 \mu^5} \left(131 \cosh(9(N - N_0)) \right. \\ &\left. + 9(2 - 2 \cosh(6(N - N_0)) + 5 \cosh(3(N - N_0))) \right). \quad (\text{A.35}) \end{aligned}$$

The expression for the imaginary part is given in the supplementary Mathematica notebook and grows as e^{-6N_0} as $N_0 \rightarrow -\infty$ whilst the real part grows as e^{-9N_0} . To obtain a finite result, we renormalise the coupling $\underline{\lambda}_3$ as

$$\lambda^2 \equiv \lim_{N_0 \rightarrow -\infty} \underline{\lambda}_3^2 e^{-9N_0}, \quad \text{so that} \quad \underline{\lambda}_3^2 = \lambda^2 e^{9N_0}. \quad (\text{A.36})$$

We arrive at the GKLS equation

$$\partial_N \rho = -i[\hat{K}_S(N), \rho] - \frac{131\pi\lambda^2 e^{6N}}{512\mu^5 \text{vol}} [\hat{\phi}, [\hat{\phi}, \hat{\rho}]], \quad (\text{A.37})$$

with system Hamiltonian given in eq. (2.3). This corresponds to standard position dephasing, with $\partial_N \rho(\phi, \phi'; N)|_{\text{diss}} = -\frac{131\pi\lambda^2 e^{6N}}{512\mu^5 \text{vol}} (\phi - \phi')^2 \rho(\phi, \phi'; N)$, which damps all off-diagonal coherences in the ϕ basis while leaving the position marginal $\rho(\phi, \phi; N)$ unchanged. Upon identifying λ with the renormalised coupling used in the main text, this expression reproduces Eq. (2.26) with the rate $\Gamma_\phi(N)$ defined there.

B Coarse graining in k -space and stochastic inflation

We coarse-grain a scalar in de Sitter to obtain the white-noise kernel for the long field, and then construct an equivalent random-Hamiltonian description. Working with $N \equiv \ln a$ and constant H , we introduce the time-dependent projector

$$\widehat{W}(k, N) = \Theta[k_c(N) - k], \quad k_c(N) = \sigma e^N H, \quad 0 < \sigma \ll 1. \quad (\text{B.1})$$

Long/short operators are defined by

$$\hat{\phi}_L(\mathbf{x}, N) = \int \frac{d^3 k}{(2\pi)^3} \widehat{W} e^{i\mathbf{k}\cdot\mathbf{x}} \hat{\phi}_{\mathbf{k}}(N), \quad \hat{\phi}_S(\mathbf{x}, N) = \int \frac{d^3 k}{(2\pi)^3} (1 - \widehat{W}) e^{i\mathbf{k}\cdot\mathbf{x}} \hat{\phi}_{\mathbf{k}}(N), \quad (\text{B.2})$$

so that $\hat{\phi} = \hat{\phi}_L + \hat{\phi}_S$. For the conjugate momentum (prime is ∂_N),

$$\hat{\pi}_{\mathbf{k}} = e^{3N} H \hat{\phi}'_{\mathbf{k}}, \quad \hat{\pi}_L(\mathbf{x}, N) = \int \frac{d^3 k}{(2\pi)^3} \widehat{W} e^{i\mathbf{k}\cdot\mathbf{x}} \hat{\pi}_{\mathbf{k}}(N). \quad (\text{B.3})$$

Differentiating the projected operators generates injection sources from shell-crossing modes,

$$\hat{\eta}_\phi(\mathbf{x}, N) = - \int \frac{d^3 k}{(2\pi)^3} (\partial_N \widehat{W}) e^{i\mathbf{k}\cdot\mathbf{x}} \hat{\phi}_{\mathbf{k}}(N), \quad (\text{B.4})$$

$$\hat{\eta}_\pi(\mathbf{x}, N) = - \int \frac{d^3 k}{(2\pi)^3} (\partial_N \widehat{W}) e^{i\mathbf{k}\cdot\mathbf{x}} \hat{\pi}_{\mathbf{k}}(N), \quad (\text{B.5})$$

with $\partial_N \widehat{W} = (\partial_N k_c) \delta(k - k_c(N))$. Below we suppress \mathbf{x} . The coarse-graining source for the field is

$$\hat{\eta}_\phi(N) = \int \frac{d^3 k}{(2\pi)^3} [-\partial_N \widehat{W}(k, N)] \hat{\phi}_{\mathbf{k}}(N). \quad (\text{B.6})$$

Using $\langle \hat{\phi}_{\mathbf{k}}(N) \hat{\phi}_{\mathbf{k}'}(N') \rangle = (2\pi)^3 \delta^{(3)}(\mathbf{k} + \mathbf{k}') |\phi_{\mathbf{k}}(N)|^2$ and converting $\delta(k_c(N) - k_c(N'))$ to $\delta(N - N')$, one finds

$$\langle \hat{\eta}_\phi(N) \hat{\eta}_\phi(N') \rangle = \frac{k_c^3(N)}{2\pi^2} |\phi_{k_c}(N)|^2 \delta(N - N'). \quad (\text{B.7})$$

For a massless scalar in de Sitter, the superhorizon mode function gives $|\phi_k(N)|^2 \simeq H^2/(2k^3)$, and evaluating on the shell $k = k_c = \sigma e^N H$ yields

$$|\phi_{k_c}(N)|^2 \simeq \frac{H^2}{2k_c^3}, \quad \Rightarrow \quad \langle \hat{\eta}_\phi(N) \hat{\eta}_\phi(N') \rangle = \left(\frac{H}{2\pi} \right)^2 \delta(N - N'), \quad (\text{B.8})$$

which is independent of σ . Defining analogously

$$\hat{\eta}_\pi(N) = \int \frac{d^3k}{(2\pi)^3} [-\partial_N \widehat{W}(k, N)] \hat{\pi}_{\mathbf{k}}(N), \quad \hat{\pi}_{\mathbf{k}} = e^{3N} H \hat{\phi}'_{\mathbf{k}}, \quad (\text{B.9})$$

one obtains

$$\langle \hat{\eta}_\pi(N) \hat{\eta}_\pi(N') \rangle = \frac{k_c^3(N)}{2\pi^2} |\pi_{k_c}(N)|^2 \delta(N - N'). \quad (\text{B.10})$$

For a massless field on superhorizon scales $\phi'_k = \mathcal{O}((k/(e^N H))^2 \phi_k)$, so on $k = k_c = \sigma e^N H$,

$$|\pi_{k_c}|^2 = e^{6N} H^2 |\phi'_{k_c}|^2 = \frac{e^{6N} H^2}{2} \mathcal{O}(\sigma^4) \frac{H^2}{k_c^3}, \quad (\text{B.11})$$

and therefore

$$\langle \hat{\eta}_\pi(N) \hat{\eta}_\pi(N') \rangle = \frac{e^{6N} H^4}{4\pi^2} \mathcal{O}(\sigma^4) \delta(N - N'). \quad (\text{B.12})$$

Since this is subleading in σ , we neglect momentum injection and retain only

$$\langle \hat{\eta}_\phi(N) \hat{\eta}_\phi(N') \rangle = \left(\frac{H}{2\pi} \right)^2 \delta(N - N'). \quad (\text{B.13})$$

We now seek a unitary stochastic evolution that reproduces (B.13) at the level of expectation values. We consider the Stratonovich stochastic Hamiltonian

$$\hat{K}_{\text{stoch}}(N) dN = \hat{K}(N) dN + \hat{L}(\hat{\phi}, \hat{\pi}_\phi; N) \circ dW, \quad \hat{L} = \hat{L}^\dagger, \quad (\text{B.14})$$

where \hat{L} is kept arbitrary for now. The unitary increment is defined by

$$d\hat{U} = -i(\hat{K} dN + \hat{L} \circ dW) \hat{U}, \quad d\hat{U}^\dagger = i\hat{U}^\dagger (\hat{K} dN + \hat{L} \circ dW), \quad (\text{B.15})$$

so that, for any operator \hat{O} , the corresponding stochastic Heisenberg equation is

$$d\hat{O} = i[\hat{K}, \hat{O}] dN + i[\hat{L}, \hat{O}] \circ dW. \quad (\text{B.16})$$

Applying (B.16) to $\hat{\phi}$ and $\hat{\pi}_\phi$ gives

$$d\hat{\phi} = i[\hat{K}, \hat{\phi}] dN + i[\hat{L}, \hat{\phi}] \circ dW, \quad d\hat{\pi}_\phi = i[\hat{K}, \hat{\pi}_\phi] dN + i[\hat{L}, \hat{\pi}_\phi] \circ dW. \quad (\text{B.17})$$

We take the system Hamiltonian to be the coarse-grained scalar Hamiltonian

$$\hat{K}(N) = \frac{e^{-3N}}{2 \text{vol } H} \hat{\pi}_\phi^2 + \frac{\text{vol } e^{3N}}{H} V(\hat{\phi}), \quad (\text{B.18})$$

for which the drift commutators are

$$i[\hat{K}, \hat{\phi}] = \frac{e^{-3N}}{\text{vol } H} \hat{\pi}_\phi, \quad i[\hat{K}, \hat{\pi}_\phi] = -\frac{\text{vol } e^{3N}}{H} V'(\hat{\phi}), \quad (\text{B.19})$$

using $[\hat{\phi}, \hat{\pi}_\phi] = i\hat{1}$. Hence the most general stochastic Heisenberg system generated by (B.14) is

$$\begin{aligned} d\hat{\phi} &= \frac{e^{-3N}}{\text{vol } H} \hat{\pi}_\phi dN + i[\hat{L}, \hat{\phi}] \circ dW, \\ d\hat{\pi}_\phi &= -\frac{\text{vol } e^{3N}}{H} V'(\hat{\phi}) dN + i[\hat{L}, \hat{\pi}_\phi] \circ dW. \end{aligned} \quad (\text{B.20})$$

Taking expectations in a normalised state yields

$$\begin{aligned} d\langle \hat{\phi} \rangle &= \frac{e^{-3N}}{\text{vol } H} \langle \hat{\pi}_\phi \rangle dN + \langle i[\hat{L}, \hat{\phi}] \rangle \circ dW, \\ d\langle \hat{\pi}_\phi \rangle &= -\frac{\text{vol } e^{3N}}{H} \langle V'(\hat{\phi}) \rangle dN + \langle i[\hat{L}, \hat{\pi}_\phi] \rangle \circ dW. \end{aligned} \quad (\text{B.21})$$

Stochastic inflation (with momentum injection neglected) requires an additive, state-independent noise of amplitude $H/2\pi$ in the ϕ equation and no noise in the π_ϕ equation. Since dW is common to all trajectories, this means that the operator coefficients themselves must satisfy

$$i[\hat{L}, \hat{\phi}] = \frac{H}{2\pi} \hat{1}, \quad i[\hat{L}, \hat{\pi}_\phi] = 0. \quad (\text{B.22})$$

The first condition implies that the commutator of \hat{L} with $\hat{\phi}$ is a c-number. For Hermitian $\hat{L}(\hat{\phi}, \hat{\pi}_\phi; N)$ this is only possible if \hat{L} is at most linear in $\hat{\pi}_\phi$ and independent of $\hat{\phi}$ up to an additive c-number, i.e.

$$\hat{L} = \alpha_1(N) \hat{\pi}_\phi + \alpha_2(N) \hat{1}. \quad (\text{B.23})$$

The second condition in (B.22) is then automatic, while the first fixes $\alpha(N) = H/2\pi$. The additive term $\ell(N)\hat{1}$ has no effect on the dynamics and may be dropped, leaving the unique choice (up to an irrelevant c-number)

$$\hat{L} = \frac{H}{2\pi} \hat{\pi}_\phi. \quad (\text{B.24})$$

Substituting (B.24) into (B.20) yields

$$\begin{aligned} d\hat{\phi} &= \frac{e^{-3N}}{\text{vol } H} \hat{\pi}_\phi dN + \frac{H}{2\pi} \hat{1} \circ dW, \\ d\hat{\pi}_\phi &= -\frac{\text{vol } e^{3N}}{H} V'(\hat{\phi}) dN, \end{aligned} \quad (\text{B.25})$$

and therefore, for expectation values,

$$\begin{aligned} d\langle \hat{\phi} \rangle &= \frac{e^{-3N}}{\text{vol } H} \langle \hat{\pi}_\phi \rangle dN + \frac{H}{2\pi} dW, \\ d\langle \hat{\pi}_\phi \rangle &= -\frac{\text{vol } e^{3N}}{H} \langle V'(\hat{\phi}) \rangle dN. \end{aligned} \quad (\text{B.26})$$

In the classical limit $\langle V'(\hat{\phi}) \rangle \simeq V'(\langle \hat{\phi} \rangle)$, and eliminating π_ϕ in the overdamped/slow-roll regime reproduces the standard stochastic-inflation Langevin equation for the coarse-grained field. Finally, for an initial pure state the corresponding Stratonovich SSE is

$$d|\psi\rangle = -i \left(\hat{K} dN + \hat{L} \circ dW \right) |\psi\rangle, \quad \hat{L} = \frac{H}{2\pi} \hat{\pi}_\phi, \quad (\text{B.27})$$

which in Itô form reads

$$d|\psi\rangle = \left(-i\hat{K} - \frac{1}{2}\hat{L}^2 \right) |\psi\rangle dN + \hat{L} |\psi\rangle dW. \quad (\text{B.28})$$

Averaging over noise realisations yields the GKLS master equation

$$\partial_N \hat{\rho} = -i[\hat{K}, \hat{\rho}] + \hat{L}\hat{\rho}\hat{L} - \frac{1}{2}\hat{\rho}\hat{L}^2 - \frac{1}{2}\hat{L}^2\hat{\rho} = -i[\hat{K}, \hat{\rho}] - \frac{1}{2} \left(\frac{H}{2\pi} \right)^2 [\hat{\pi}_\phi, [\hat{\pi}_\phi, \hat{\rho}]], \quad (\text{B.29})$$

i.e. a single $\hat{\pi}_\phi$ Lindblad operator implementing stochastic translations in ϕ .

C Adiabatic theorem for an oscillator in de Sitter

Consider the time-dependent quadratic Hamiltonian

$$K_S(t) = \frac{\pi_\phi^2}{2e^{3Ht}} + \frac{e^{3Ht}}{2} m^2 \phi^2, \quad (\text{C.1})$$

with $N \equiv Ht$. This can be written in the general form of a parametric oscillator,

$$\hat{K}_S(t) = \frac{\hat{\pi}^2}{2M(t)} + \frac{M(t)}{2} \omega^2 \hat{\phi}^2, \quad \text{where } M(t) = e^{3Ht}, \quad \omega = m. \quad (\text{C.2})$$

The time derivative in the Schrödinger picture is

$$\dot{K}_S(t) = -\frac{\dot{M}}{2M^2} \hat{\pi}^2 + \frac{\dot{M}}{2} \omega^2 \hat{\phi}^2 = \frac{\dot{M}}{2M} \omega (\hat{a}^2 + \hat{a}^{\dagger 2}), \quad (\text{C.3})$$

where \hat{a} and \hat{a}^\dagger are the instantaneous ladder operators associated with $M(t)$ and ω . A sufficient condition for adiabatic evolution is given in [78] as

$$\frac{|\langle m(t) | \dot{K}_S(t) | n(t) \rangle|}{[E_n(t) - E_m(t)]^2} \ll 1 \quad \text{for all } m \neq n, \quad (\text{C.4})$$

Where n and m are labelling the eigenstates with energies E_n and E_m . The nonvanishing matrix elements of \dot{K}_S occur only between states differing by two quanta. Evaluating these gives the adiabatic parameters

$$\frac{|\langle n+2 | \dot{K}_S | n \rangle|}{(E_n - E_{n+2})^2} = \frac{3H}{8m} \sqrt{(n+1)(n+2)}, \quad \frac{|\langle n-2 | \dot{K}_S | n \rangle|}{(E_n - E_{n-2})^2} = \frac{3H}{8m} \sqrt{n(n-1)}, \quad (\text{C.5})$$

and zero for all other $m \neq n$. In particular, the ground-state (vacuum) mixing parameter is

$$\frac{|\langle 2 | \dot{K}_S | 0 \rangle|}{(E_0 - E_2)^2} = \frac{3\sqrt{2}}{8} \frac{H}{m}. \quad (\text{C.6})$$

Hence, the evolution is adiabatic provided that

$$\frac{m}{H} \gg 1. \quad (\text{C.7})$$

D Additional simulations

To keep the main text concise, we omitted several simulation results that are not essential for understanding the effects of non-adiabatic dynamics, decoherence, and false-vacuum populations. In this appendix, we present a selection of these additional simulations.

D.1 $\phi^2 \chi^2$ four point interactions

We also investigated a \mathbb{Z}_2 -symmetric stochastic unraveling in which the environment couples quadratically to the spectator field, leading to the nonlinear SSE

$$d|\psi\rangle = -i\hat{K}_S|\psi\rangle dN - \frac{\pi\lambda^2 e^{6N}}{64\mu^4} \left(\hat{\phi}^2 - \langle \hat{\phi}^2 \rangle \right)^2 |\psi\rangle dN + \frac{\lambda e^{3N}}{4\mu^2} \sqrt{\frac{\pi}{2}} \left(\hat{\phi}^2 - \langle \hat{\phi}^2 \rangle \right) |\psi\rangle dW, \quad (\text{D.1})$$

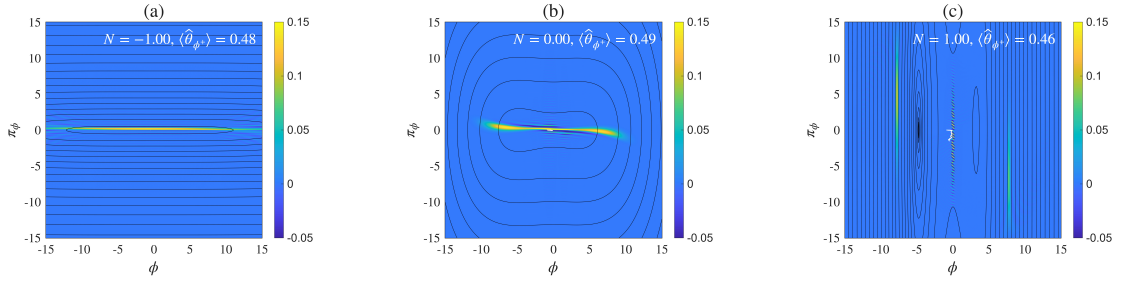


Figure 10: Wigner functions for the \mathbb{Z}_2 symmetric SSE evolution Eq. (D.1). The columns correspond to different snapshot times. Black curves are equal-energy contours of $K_S(N)$. Axes are ϕ and π_ϕ . In-panel text reports the e -fold N and the false vacuum projector expectation value. The sonified video corresponding to these plots is available [via this link](#). The white line corresponds to the prior evolution of the phase space expectation values $\langle \hat{\phi} \rangle$ and $\langle \hat{\pi}_\phi \rangle$.

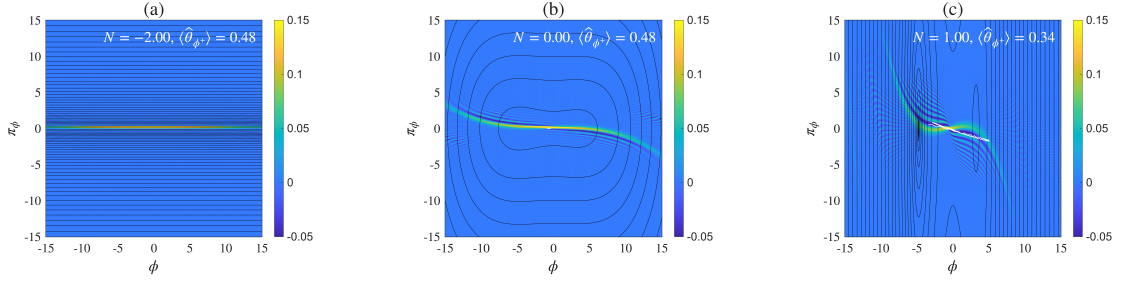


Figure 11: Wigner functions for the NMQSD (Eq. (D.2)) trajectory with coupling $\lambda_3 = 100$ and spectator frequency $\omega_\chi = 10$. Columns correspond to different snapshot times. Black curves are equal-energy contours of $K_S(N)$. Axes are ϕ and π_ϕ . In-panel text reports the e -fold N and the false vacuum projector expectation value. The sonified videos corresponding to these plots are available via these links: [this link](#). The white line corresponds to the prior evolution of the phase space expectation values $\langle \hat{\phi} \rangle$ and $\langle \hat{\pi}_\phi \rangle$.

with Lindblad operator proportional to $\hat{\phi}^2$. In contrast to the $\hat{L} \propto \hat{\phi}$ channel discussed in the main text, this \mathbb{Z}_2 -symmetric dynamics dephases in the $\hat{\phi}^2$ pointer basis and therefore preserves the $\phi \rightarrow -\phi$ symmetry: superpositions of states with opposite sign but equal magnitude of ϕ are not distinguished by the bath. As a result, the ϕ^2 -coupled environment efficiently suppresses coherences between configurations with different $|\phi|$, but it does not by itself drive vacuum selection between the true and false minima in an asymmetric double well. This behaviour is clearly visible in the Wigner snapshots of Fig. 10, where the state becomes strongly mixed and increasingly classical in $|\phi|$ while retaining approximate symmetry between positive and negative field values, in marked contrast to the $\hat{L} \propto \hat{\phi}$ trajectories that rapidly localize into a single well.

D.2 Non-Markovian single spectator environment

A convenient way to realise a genuinely non-Markovian dynamics is to couple the spectator field to a *single* massive environment field χ via the cubic interaction $\phi\chi^3$, and then apply the non-Markovian quantum state diffusion (NMQSD) formalism of Diósi, Gisin and Strunz [79, 80]. In this case the

reduced dynamics of the system field is unraveled by the nonlinear, norm-preserving NMQSD equation,

$$\frac{\partial}{\partial N} |\psi(z^*)\rangle = \left(-i\hat{K}_S(N) + \frac{\lambda e^{3N}}{H} (\hat{\phi} - \langle \hat{\phi} \rangle) z_N^* - \frac{\lambda e^{3N}}{H} (\hat{\phi} - \langle \hat{\phi} \rangle) \int_{N_0}^N d\bar{N} C(N, \bar{N}) \frac{\delta}{\delta z_{\bar{N}}^*} \right) |\psi(z^*)\rangle, \quad (\text{D.2})$$

where $z_N \equiv z(N)$ is a complex Gaussian process with zero mean and coloured correlations

$$\mathbb{E}[z_N] = 0, \quad \mathbb{E}[z_N z_{\bar{N}}] = 0, \quad \mathbb{E}[z_N z_{\bar{N}}^*] = C(N, \bar{N}). \quad (\text{D.3})$$

The same kernel $C(N, \bar{N})$ therefore governs both the non-local memory term and the noise correlations.

The non-local memory kernel $C(N, \bar{N})$ is fixed by the spectator-field correlators. Writing the total interaction as $\hat{H}_{\text{int}}(N) = \tilde{\lambda}_3 \hat{\phi} \hat{\chi}_I^3(N)$, one finds

$$C(N, \bar{N}) = \tilde{\lambda}_3^2 \left(\langle 0_{N_0} | \hat{\chi}_I^3(N) \hat{\chi}_I^3(\bar{N}) | 0_{N_0} \rangle - \langle 0_{N_0} | \hat{\chi}_I^3(N) | 0_{N_0} \rangle \langle 0_{N_0} | \hat{\chi}_I^3(\bar{N}) | 0_{N_0} \rangle \right). \quad (\text{D.4})$$

Applying the renormalization scheme in Eq. (A.36) yields a stationary correlator that depends only on the e-fold difference $\Delta N = N - \bar{N}$,

$$C(N, \bar{N}) = \frac{3\lambda_3^2}{128 H^3 \omega_\chi^3} \left[9 \cos(\omega_\chi \Delta N) + \cos(3\omega_\chi \Delta N) \right], \quad \omega_\chi \equiv \frac{m_\chi}{H}, \quad (\text{D.5})$$

so that (D.4) provides an explicit non-local kernel $C(N, \bar{N})$ for use in the NMQSD equation and the corresponding non-Markovian master equation. In the the Wigner snapshots of Fig. 11 we can see that the periodic non-Markovian driving can lead to periodic transitions between vacua.